Ore Geology Reviews 159 (2023) 105529

Contents lists available at ScienceDirect

Ore Geology Reviews

journal homepage: www.elsevier.com/locate/oregeorev

Ore-forming processes of the Baisong carbonate-hosted Pb-Zn deposit, SW China: Constraints from in-situ sphalerite trace element and sulfide S-isotopic compositions

Shiyu Liu [a], Lin Ye [b,*], Ruidong Yang [a,*], Zhenzhong Xiang [b,c], Chen Wei [b,c], Yusi Hu [b], Zhilong Huang [b], Sichen Liu [b,c]

[a] College of Resources and Environmental Engineering, Guizhou University, Guiyang 550025, China
[b] State Key Laboratory of Ore Deposit Geochemistry, Institute of Geochemistry, Chinese Academy of Sciences, Guiyang 550081, China
[c] University of Chinese Academy of Sciences, Beijing 100049, China

ARTICLE INFO

Keywords:
Sphalerite
In-situ trace elements and S isotopes
Western Hunan-eastern Guizhou Pb-Zn ore belt
Baisong Pb-Zn deposit
Mississippi Valley-Type (MVT) deposits

ABSTRACT

The western Hunan-eastern Guizhou (WHEG) Pb-Zn ore belt in the southwestern Yangtze block is a main Pb-Zn province in China. The metallogenic characteristics of this ore belt were widely reported, but the ore-forming process is still poorly understood. The lower Cambrian carbonate-hosted Baisong deposit is a representative Pb-Zn deposit in the southern WHEG belt. Sphalerite trace elements and sulfur isotopic compositions from the Baisong Pb-Zn deposit could reveal the ore-forming fluid source and metallogenic processes. Four types of sphalerites have been distinguished (black colloidal sphalerite (Sp) I, light-colored sector Sp II, red zoned Sp III and brown zoned Sp IV, indicating four sulfide mineralization stages from the early ore phase. Sp I (66-117℃, $\delta^{34}S$: +24.8 to + 27.8‰) has the highest Cd-Ga-Ag-Cu contents among the four sphalerite types, and commonly overgrow with marcasite. This suggests that Sp I was formed from acidic fluids under high precipitation rate. The trace elements and sulfur isotopic compositions of Sp II (80-128℃, $\delta^{34}S$: +26.5 to + 28‰) are similar to Sp I. Sp II was likely formed by a decrease in oversaturation and precipitation rate with fluid pH increase. Sp III (127-164℃, $\delta^{34}S$: +31 to + 32.5‰), commonly overgrow on pyrite (Py I), has higher Mn-Fe-Ge but lower Cd-Cu-Ga-Ag contents and heavier sulfur isotopes than Sp II. Changes in precipitation environment and fluid compositions are likely major factors in forming Sp III (temperature increase, pH increase and more reduced). The forming of Sp III and Py I likely consumed the Fe and Ge in the fluid, depriving those elements from the later-formed Sp IV (97-141℃, $\delta^{34}S$: +25.7 to + 29.8‰). The sulfide $\delta^{34}S$ value (+22.5 to + 46.3‰) implies that the S^{2-} at Baisong was sourced from seawater sulfates via thermochemical sulfate reduction (TSR). Sphalerite trace element features reflect that the Baisong is an MVT deposit.

1. 1.Introduction

Sphalerite occurs in various textures, such as colloform and concentric zoned (McLimans et al., 1980; Pattrick et al., 1993; Barrie et al., 2009). These textures in Mississippi Valley-type (MVT) ores (Barton et al., 1977; Di Benedetto et al., 2005; Barrie et al., 2009; Belissont et al., 2014, Wei et al., 2021) indicate sequential hydrothermal fluid evolution (Wei et al., 2021) and record the physicochemical conditions during mineral precipitation (Pattrick et al., 1993). Sphalerite is a key ore mineral in Pb-Zn deposits and can host a variety of trace elements (incl. Fe, Mn, Cd, In, Ge, Ag and Ga), which are widely used to discriminate ore deposit types and reveal any changes in fluid physicochemical conditions (Belissont et al., 2014; Cook et al., 2009; Di Benedetto et al., 2005; Frenzel et al., 2016; Ye et al., 2011). Sulfur isotopes of ore sulfides would help to resolve issues such as the sulfur source and precipitation mechanism (Rye and Ohmoto, 1974; Zhou et al., 2018a; Zhou et al., 2018b). Integrating sphalerite trace element and sulfur isotopic compositions would provide a proxy for the origin and nature of ore fluids and ore-forming processes (Anderson, 1983; Corbella et al., 2004).

The WHEG Pb-Zn ore belt, located in southeastern margin of the Yangtze plate, is mainly hosted in Cambrian carbonate platforms (Hu

* Corresponding authors.
E-mail addresses: yelin@vip.gyig.ac.cn (L. Ye), rdyang@gzu.edu.cn (R. Yang).

https://doi.org/10.1016/j.oregeorev.2023.105529
Received 4 February 2023; Received in revised form 30 May 2023; Accepted 2 June 2023
Available online 7 June 2023

and Zhou, 2012). About 200 Pb-Zn deposits of different sizes were discovered in the belt, hosting a total sulfide ore resource of > 300 Mt (Wei et al., 2017). From north to south, major Pb-Zn deposits in the belt include the Limei, Yutang, Xiunao, Baisong, Niujiaotang (Hu et al., 2020a; Hu et al., 2020b). Many studies on the ore belt were dedicated to understand its geology (Huang et al., 2004; Duan, 2014), geochronology (e.g., Duan, 2014; Tan et al., 2018), S-Pb isotopes (Hu et al., 2022), and fluid inclusions (e.g., Liu and Zheng, 2000; Zhou et al 2018c). Previous studies showed that the WHEG Pb-Zn mineralization resembles Mississippi Valley-type (MVT). MVT deposits have diverse ore geological characteristics (Leach et al., 2010), and many contain economic endowment of high-tech metals such as Ge and Ga (Luo et al., 2022). Although the metallogenic features of MVT deposits were widely concerned (Schneider et al., 2002), the ore-forming process is poor understanding and still should deeply researched (Zhou et al., 2022).

In the southern WHEG Pb-Zn ore belt, the Baisong Pb-Zn deposit has a simple metallic sulfide assemblage (incl. sphalerite, galena and pyrite). Previous metallogenic studies are rare (Huang, 2003), which limit the understanding of Pb-Zn mineralization of the belt. Our latest research shows that the Baisong deposit has four textural types of sphalerites, and the sphalerite shows Ge enrichment. Thus, the Baisong Pb-Zn deposit offers a good target to investigate the trace element and S isotope geochemistry of different types of sphalerites. Here, we analyzed the sphalerite trace element geochemistry and sphalerite and pyrite sulfur isotopes through laser ablation inductively coupled plasma mass spectrometry (LA-ICP-MS), with the aim to determine the ore-forming mechanism and the ore-material source for the WHEG carbonate-hosted Pb-Zn ores.

2. Geologic setting

2.1. Regional geology

The Yangtze Block (part of the South China Block) is bounded by the Qinling-Dabie, Songpan-Ganzê, Sanjiang and Cathaysia terranes, in the north, northwest, west and southeast, respectively (Fig. 1a). It consists of a upper Paleoproterozoic to lower Neoproterozoic crystalline basement composed of *meta*-sandstone–siltstone and silty slate, and is covered by upper Ediacaran to Quaternary sequences (Metcalfe, 2006). The Yangtze Block has experienced multiple tectonic events (Metcalfe, 2006; Charvet, 2013), including the Neoproterozoic (850–820 Ma) Jiangnan Orogen formed by the Yangtze-Cathaysia collision (Zhao et al., 2011), the early Paleozoic Wuyi-Yunkai intracontinental orogeny (490–410 Ma), and the Nanhua rifting that developed a foreland basin (Yao and Li, 2016).

In the WHEG Pb-Zn ore belt, the oldest unit is the upper Proterozoic Banxi Group slate with minor low-grade metamorphosed sandstone and carbonates. The Paleozoic-Quaternary sequences are composed of carbonates, shales and argillaceous sandstones, but middle-upper Silurian sequences are missing (Zhao et al., 2011; Zhao, 2015; Zhou et al., 2018b; Wang et al., 2018).

The lower-middle Cambrian to lower Ordovician carbonate platform sequences are the primary sulfide hosts in the area. Over 300 Pb-Zn deposits of various sizes are hosted by the lower Cambrian Qingxudong Formation and minor in the upper Ediacaran to Ordovician rocks (Fig. 1b). Four major NNE-/NE-trending regional faults (incl. the Yinjiang–Huayuan, Songtao-Zhangjiajie, Kaili–Xinhuang–Zijiang, and the Baojing–Tongren–Yuping) controlled the distribution of the WHEG Pb-Zn deposits (Li et al., 2010; Wang et al., 2013), including the Niujiaotang, Baisong, Banbianjie deposits and the Huayuan orefield (Ye et al.,

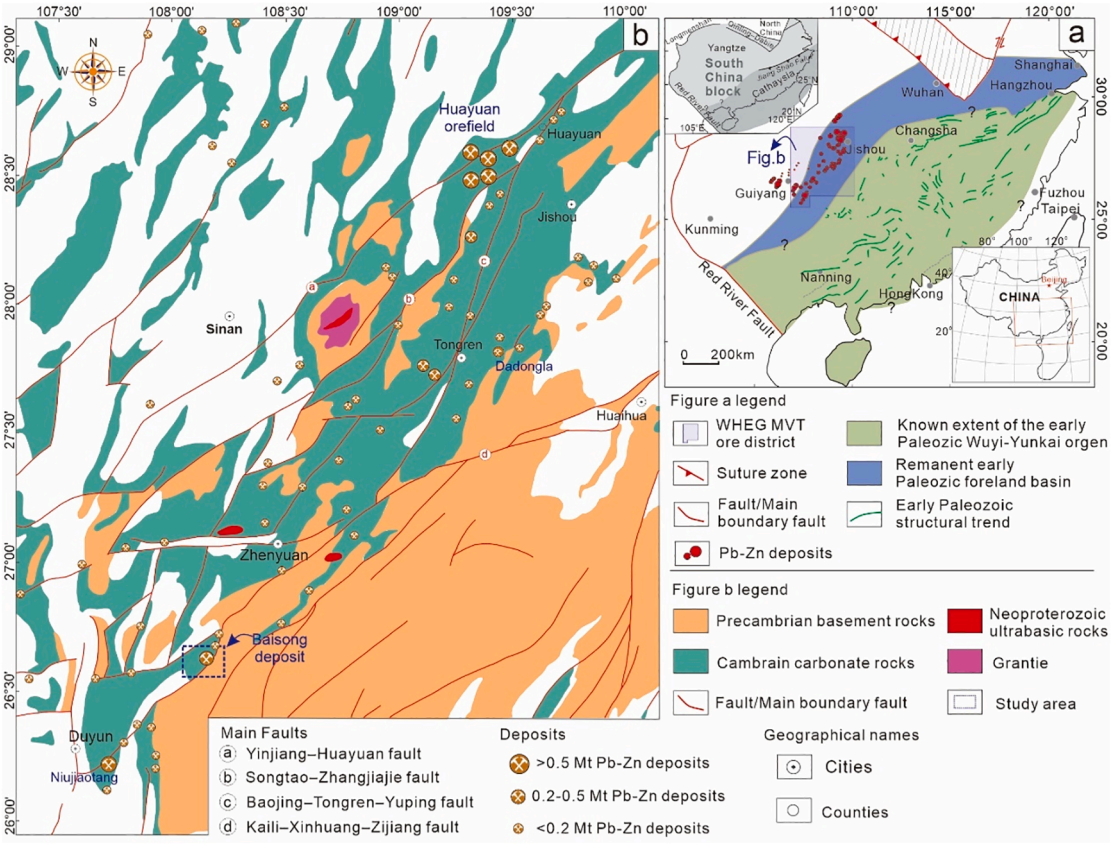

Fig. 1. (a) Simplified regional map of South China, highlighting the regional extent of the early Paleozoic Wuyi–Yunkai orogeny and carbonate-hosted Pb-Zn deposits in the western Hunan–eastern Guizhou metallogenic belt (modified from Li et al., 2010); (b) Geological map of the western Hunan–Eastern Guizhou district, showing the distribution of Pb-Zn deposits, strata, and regional faults (modified from Li, 2018).

2011; Huang, 2003; An et al., 2022; Hu et al., 2022).

2.2. Ore deposit geology

The Baisong Pb-Zn deposit in the southern WHEG belt have similar geological characteristics to those of Niujiaotang deposit in Duyun (Fig. 1). The exposed stratigraphy (from bottom to top) are the mid-lower Cambrian Qingxudong, Gaotai, Shilengshui Formations (Fig. 2a). The middle Cambrian Shilengshui Formation has two members: (1) fine-grained dolomite, oolitic dolomite and terrestrial clastic-bearing dolomite; and (2) sandy/silty dolomite above fine-grained (oolitic) dolomite (Huang, 2003). The lower Cambrian Qingxudong Formation has three members: (1) carbonaceous/argillaceous dolomite; (2) laminated dolomite intercalated with zebra dolomite; and (3) fine-grained dolomite and argillaceous dolomite (Jin et al., 2016). The Qingxudong Formation and the Shilengshui Formation are the host rocks (Fig. 2b). The dominant faults are the NE-/NEE-trending longjingjie, dagechong and jindongsi thrust faults (Fig. 2a; Huang, 2003).

2.2.1. Sulfide mineralization and alteration

Sulfide mineralization is stratiform (Fig. 3a-b) or lenticular (Fig. 3c), and locally veined or massive (Fig. 3d) in the Qingxudong and Shilengshui Formations. Each of the three main orebodies is ~ 2500 m-long and 2.5 to 5 m-thick (max. 8 m-thick), with about 30 m and 55 m vertical separation in-between. Orebody I is the largest, whereas orebody II and III are relatively small. Orebody I contains > 0.3 Mt ore at 4–8% Pb + Zn. The lenticular orebodies are average ca. 1.2–8 m thick, 2500 m long and 10–25 m wide. Orebody II is ca. 8000 m long, 10–25 m wide, and 1.2–6 m thick, and has 3–6% Zn and 1.5% Pb. Orebody III is ca. 800 m long, 10–25 m wide and 1.2–3 m thick, and has 3.35% Zn and 1.5% Pb (Huang, 2003).

Wall-rock alterations at Baisong include dolomite (dominant) and calcite (Figs. 3 and 4). Dolomite alteration occurred widely in the Qingxundong and Shilengshui Formations, and shows a close spatial relation with the Zn-Pb mineralization (Fig. 3a-f).

2.2.2. Mineralogy and paragenesis

Metallic minerals at Baisong include mainly sphalerite, galena, and pyrite, and minor marcasite, cerussite, and masicotite. Dolomite is the main non-metallic minerals (Figs. 3 and 4). According to the mineral assemblages and paragenetic relationship (Figs. 3 and 4), the alteration and mineralization comprise three stages (Fig. 5), i.e., (1) sedimentary diagenesis, (2) hydrothermal mineralization (incl. an early and a late stage), (3) supergene oxidization. Four types of sphalerites were formed in the early ore stage: Black colloidal sphalerite (Sp I) is often porous and associated with marcasite (Fig. 4a-b); Light-colored sector-zoned sphalerite (Sp II) intergrowth with Sp I (Fig. 4a-c); Reddish and zoned sphalerite (Sp III) intergrowth with Sp II; Brown zoned sphalerite (Sp IV) intergrowth with Sp III (Fig. 4d-e). Notably, Sp III is commonly associated with pyrite (Py I), and is much rarer than other three types of sphalerites. Late-ore stage: Galena and granular pyrite (Py II) were generally formed on the margin of sphalerite or replaced it, suggesting that Pb mineralization occurred after Zn mineralization (Fig. 4g-i).

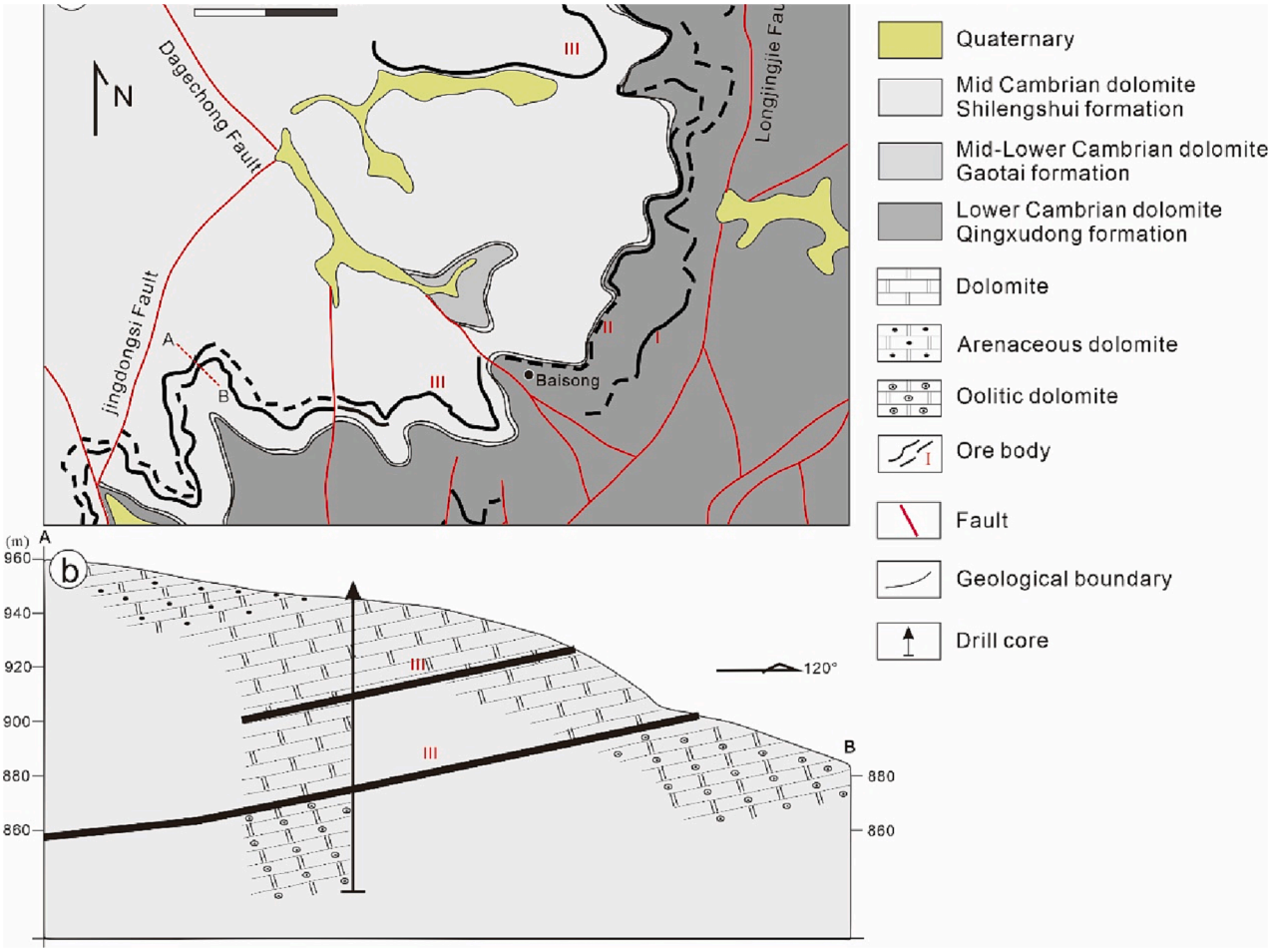

Fig. 2. (a) Geological sketch map of the Baisong district, showing the distribution of ore blocks, strata, and faults; (b) Geological profile A-B at Baisong, showing the distribution of orebodies, faults and strata (modified from Huang, 2003).

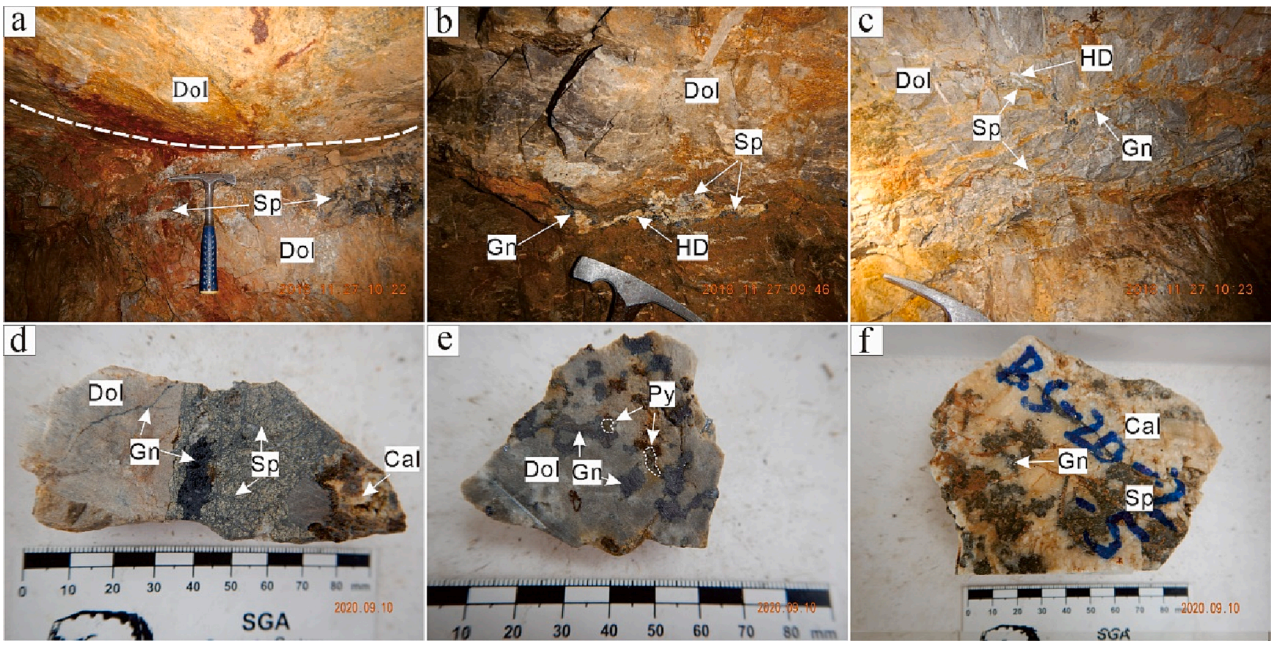

Fig. 3. Photographs of field and hand-specimens from the Baisong deposit: (a) Stratiform orebody; (b) Hydrothermal dolomite vein orebody; (c) Hydrothermal vein orebodies cut wallrock; (d) Massive sphalerite-galena ore associated with dolomite; (e) Disseminated galena and pyrite in dolomite; (f) Disseminated galena and pyrite in calcite. Abbreviations: Sp-sphalerite, Py-pyrite, Gn-galena, Dol-dolomite, Cal-calcite, HD- Hydrothermal dolomite.

3. Samples and analysis methods

3.1. Sampling and sample preparation

In this study, 100 representative samples were obtained from outcrops of the Baisong mine. Among them, nine representative sphalerite samples were prepared for in-situ LA-(MC-)ICP-MS trace element and S isotope analyses. Standard polished thin sections (~100 μm) were prepared for ore microscopy. All of the following analyses were carried out at the State Key Laboratory of Ore Deposit Geochemistry, Institute of Geochemistry, Chinese Academy of Sciences (IGCAS).

3.2. SEM-EDS and LA-ICP-MS

Scanning electron microscope (SEM) analysis was conducted on a JSM-7800F Field Emission SEM (Japan), coupled with an EDAX TEAM Apollo XL energy-dispersive spectroscope (EDS) and the TAEM software (UK).

For the analysis of LA-ICP-MS trace element, laser ablation was carried out on an ASI RESOLution-LR-S155 laser microprobe, fitted with a Coherent Compex-Pro 193 nm ArF excimer laser. An Agilent 7700x ICP-MS instrument was used to acquire ion-signal, and helium (350 ml/min) was used as a carrier gas. The ablated aerosol was mixed with Ar make-up gas (900 ml/min) before leaving the cell. The analyses were carried out with 26 μm spot size, 5 Hz pulse frequency and 3 J/cm^2 energy fluence. STDGL3 was used as a standard for chalcophile and siderophile elements (Danyushevsky et al., 2011). The recommen1ded element concentrations for the USGS reference glasses are from the GeoReM database (https://georem.mpch-mainz.gwdg.de/). The sulfide MASS-1 standard was analyzed as an unknown to check the analytical accuracy.

3.3. Sulfur isotope analysis

The analysis was conducted on a Nu Plasma III MC-ICP-MS (Nu Instruments) connected to a RESOlution-155 ArF193-nm laser ablation system (Australian Scientific Instruments). The mass separation was calculated at 0.3333. The instrument was set to pseudo-medium resolution mode (Millet et al., 2012) to resolve polyatomic interference from ^{16}O-^{16}O for ^{32}S and ^{16}O-^{18}O for ^{34}S. The source slot was adjusted to medium (0.05 mm), in combination with the use of the alpha slot. Sulfide was ablated in a mixed nitrogen (2 ml/min) and helium (350 ml/min) atmosphere using the following parameters: 40–60 μm spot size, 40 s wash time, 20 s baseline time, 40 s ablation time, 2–3 J/cm^2 energy density, and 5 Hz repetition rate. All the analyses followed the standard procedures of analyzing one standard pyrite powder tablet (PSPT-2) for every three samples (Bao et al., 2017; Chen et al., 2019). Two internal standards of natural pyrite crystals (SB-1 from Shangbao W-Sn deposit and HYC-1 from Huayangchuan Nb-U-REE deposit, China) were analyzed for quality control. The measured $\delta 34_{SV\text{-}CDT}$ value is −5.76‰ for HYC-1 (n = 12) and 16.57‰ (n = 12) for SB-1, consistent with the recommended value (16.57‰ for SB-1 and −5.76‰ for HYC-1) (IRMS).

4. Results

4.1. Trace element compositions in sphalerite

Trace element compositions of the four sphalerite types are summarized in Table 1 and illustrated in Fig. 6 (n = 32 (Sp I), 53 (Sp II), 3 (Sp III), and 11 (Sp IV); ESM 1).

Contents of Fe (795–40756 ppm, mean 6147 ppm) and Cd (254–16731 ppm, mean 5070 ppm) contents are high in sphalerite. The sphalerite has also relatively high Ge (111–747 ppm, mean 244 ppm) and Pb (174–1965 ppm, mean 395 ppm) contents. Some grains have over 100 ppm Cu and Ag, whose contents are generally 0.33 to 220 ppm (mean 16.7 ppm) and 0.30 to 162 ppm (mean 11.9 ppm), respectively. Contents of other trace elements are mostly < 10 ppm, for instance Mn (0.43–16.1 ppm, mean 3.92 ppm). Ga (0.02–46.3 ppm, mean 6.33 ppm), and Tl (1.95–29.7 ppm, mean 6.97 ppm).

It is noteworthy that trace element contents change regularly from Sp I to Sp IV, with the Mn, Fe, Ge and Tl contents show an increasing trend, while the Cu, Ga, Ag and Cd contents show an decreasing trend (Fig. 6).

4.2. Sulfur isotopic compositions

Sulfur isotopic compositions determined by LA-MC-ICP-MS are listed

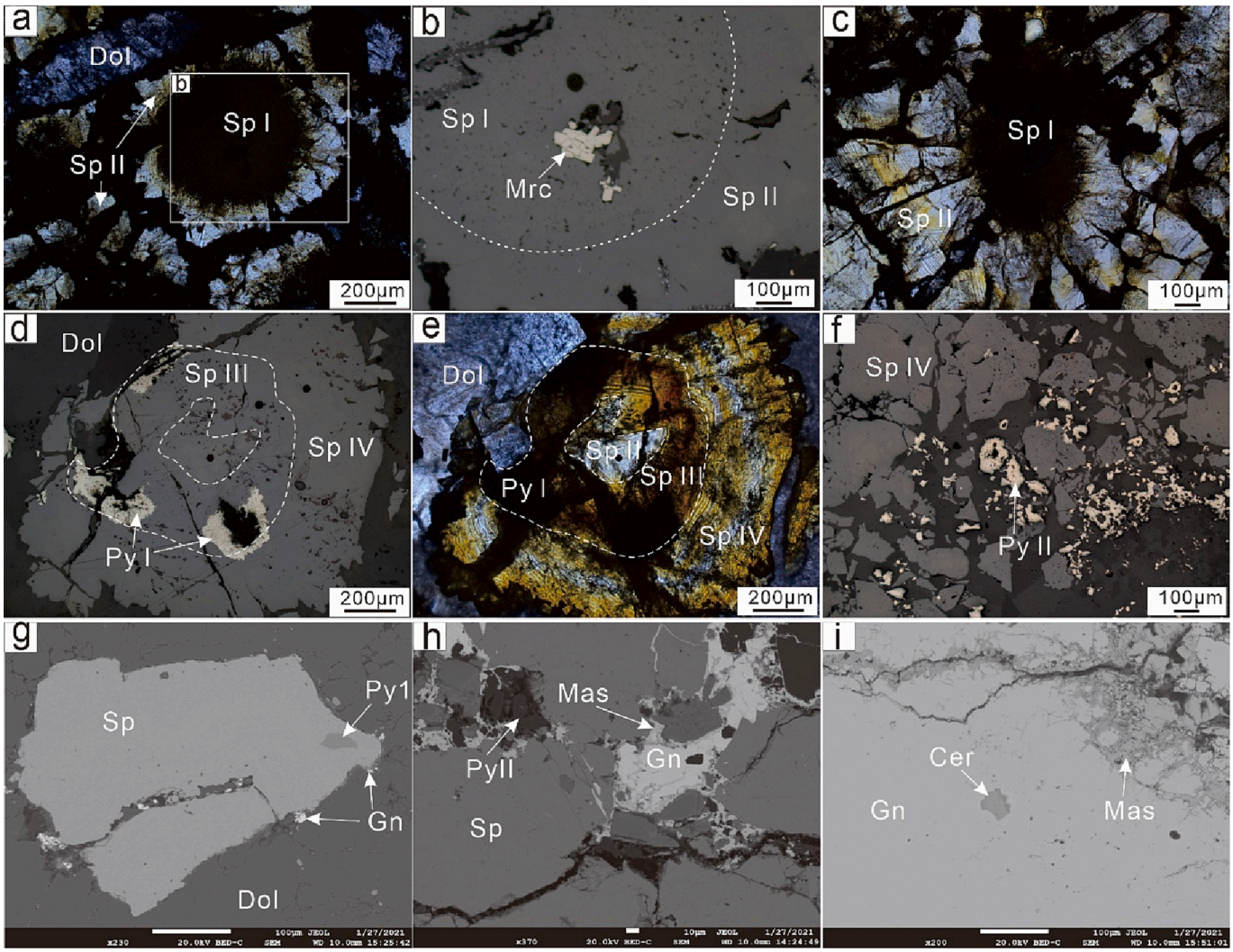

Fig. 4. Photomicrographs of hydrothermal mineral textures in the Baisong deposit: (a-c) Black colloidal sphalerite (Sp I) associated with light-colored sector sphalerite (Sp II); (b) Marcasite in Sp I; (d-e) Zoned red sphalerite (Sp III) associated with pyrite (Py I) and Sp II and zoned (intergrowth) brown sphalerite (Sp IV); (f) Sp IV and granular pyrite (Py II); (g) Galena on sphalerite margin (BSE image); (h) Galena and Py II replaced sphalerite, masicotite intergrowth galena; (i) Galena associated with cerussite and masicotite. Abbreviations: Sp-sphalerite, Py-pyrite, Gn-galena, Mrc- marcasite, Cer-Cerussite, Mas-masicotite, Dol-dolomite, Cal-calcite, HD-hydrothermal dolomite. (For interpretation of the references to color in this figure legend, the reader is referred to the web version of this article.)

in Table 2 and presented in Fig. 7. $\delta^{34}S$ values are + 24.8 to + 27.8‰ for Sp I (n = 4; mean + 25.9‰), +26.5 to + 28‰ for Sp II (n = 4; mean + 27‰), +31 to + 32.5‰ for Sp III (n = 3; mean + 31.7‰), +25.7 to + 29.8‰ for Sp IV range (n = 3; mean + 28‰), +34.2 to + 46.3‰ for Py I (n = 3; mean + 34.7‰), and + 22.5 to + 30.1‰ for Py II (n = 5; mean + 26.7‰).

5. Discussion

5.1. Occurrence of trace elements in sphalerite

5.1.1. Relations between color and geochemical compositions

Trace element incorporation in sphalerite is correlated with the sphalerite color. Previous studies considered that the sphalerite color is largely attributed to the Fe substitution for Zn in the sphalerite lattice, but other elements (e.g., Mn, Co) can also influence on the color (L'Heureux, 2000; Barrie et al., 2009; Cook et al., 2009). Previous studies on MVT sphalerite suggested that the color of colloform sphalerite is strongly correlated with As content (rather than Fe) (Pfaff et al., 2011; Gagnevin et al., 2012). For the Baisong sphalerite, the As content in the different color zones are mostly below the detection limit, suggesting that the color is unlikely controlled by the As content. It is noteworthy that four types of Baisong sphalerite have significantly different Fe contents. The black colloform sphalerite (Sp I) have the lowest Fe contents (mean 0.48 wt%) while the red zoned sphalerite (Sp III) has the highest Fe contents (mean 2.87 wt%). Iron content is higher than that of other trace elements in the Baisong sphalerite, and a well-defined correlation between Fe content and sphalerite color is present. This phenomenon is also reported by the color-zoned sphalerite from the Dadongla Zn-Hg deposit and Nayongzhi Pb-Zn deposit in South China, where high Fe content is correlated with brown color (Hu et al., 2020a; Hu et al., 2020b; Wei et al., 2021).

5.1.2. Trace elements substitution in sphalerite

Representative time-resolved depth profiles (Fig. 8) show smooth and flat signal spectra for Mn, Fe, Cd, Ge, Tl and Ga, suggesting that these elements likely occur as solid solution or homogenously-distributed nanoparticles (Gregory et al., 2014; Hu et al., 2020a; Hu et al., 2020b).

Bivalent cation (Cu^{2+}, Fe^{2+}, Mn^{2+} and Cd^{2+}) have similar ionic radius to that of Zn^{2+}. These ions are largely incorporated in sphalerite via direct substitution for Zn^{2+}($M^{2+} \leftrightarrow Zn^{2+}$; Cook et al., 2009; Ye et al.,

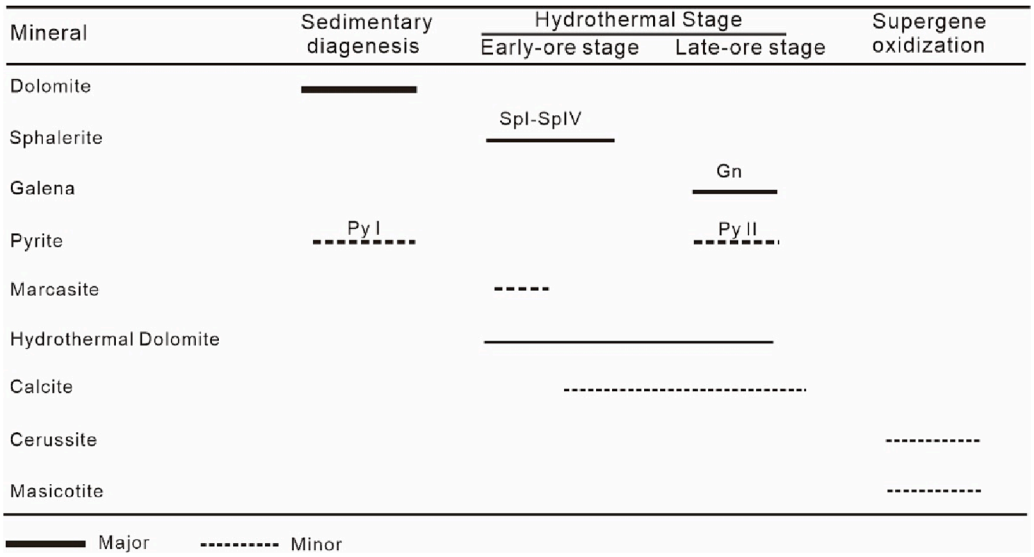

Fig. 5. Mineral assemblages and paragenetic sequence of the Baisong deposit.

Table 1
LA-ICP-MS results for the different sphalerite species (ppm).

Sample		Mn	Fe	Co	Ni	Cu	Ga	Ge	Ag	Cd	Tl	Pb	Zn	Se
Sp I	**Mean**	4.25	4774	1.71	0.15	29.2	12.3	210	20.3	6259	5.71	454	661,025	0.47
($n = 32$)	**Min**	1.35	795	0.02	0.07	0.33	0.03	117	0.75	406	1.95	174	655,197	0.17
	Max	11.4	10,397	5.02	0.48	220	46.3	418	162	16,731	13.9	824	665,942	1.19
Sp II	**Mean**	3.21	5635	1.82	0.14	13.4	4.22	228	9.64	4687	6.36	324	661,499	0.63
($n = 54$)	**Min**	0.43	1494	0.02	0.08	0.36	0.02	111	0.75	382	1.97	177	649,574	0.17
	Max	7.66	18,472	5.98	0.41	185	33.1	416	121	13,381	14.5	864	665,527	2.02
Sp III	**Mean**	11.1	26,947	0.26	0.13	1.32	2.25	548	1.30	723	22.7	623	638,561	5.44
($n = 13$)	**Min**	8.1	9065	0.02	0.00	0.24	0.02	404	0.30	254	17.0	303	623,120	0.18
	Max	16.1	40,756	0.51	0.31	5.36	6.42	747	2.41	1584	29.7	1965	656,175	9.72
Sp IV	**Mean**	3.78	6494	0.13	0.13	0.63	0.81	338	1.13	4724	9.75	387	660,584	1.05
($n = 11$)	**Min**	0.91	1355	0.02	0.11	0.38	0.03	116	0.74	650	3.02	177	652,986	0.18
	Max	10.1	17,005	0.99	0.17	2.26	2.82	682	2.26	10,039	26.4	943	663,877	1.35

2011; Murakami and Ishihara, 2013; Hu et al., 2020a; Hu et al., 2020b and reference therein). Strong negative Fe vs. Cd correlation suggests direct substitution of (Fe^{2+}, Cd^{2+}) ↔ Zn^{2+} for the Baisong sphalerite (Fig. 9a). Copper in sphalerite occurs mainly as chalcopyrite inclusions or as solid solution by the substitution of Zn^{2+} (Barton and Bethke, 1987). At Baisong, detailed optical and SEM petrographic observations have not found any chalcopyrite inclusions (Fig. 4), and the positive Cu vs. Ag correlation (Fig. 9b) suggests that Cu^{+} and Ag^{+} provide charge compensation for the di-, tri- or tetravalent cations (In^{3+}, Ga^{3+} and Sn^{4+}) substitution for Zn (Cook et al., 2009; Ye et al., 2011). Meanwhile, there is no correlation between (Cu + Ag) and Ge (Fig. 9c), indicating that the Ge corporation in sphalerite was not caused by $2(Cu, Ag)^{+}+Ge^{4+} \leftrightarrow Zn^{2+}$. The coupled substitution $(Cu, Ag)^{+} + Ga^{3+} \leftrightarrow 2Zn^{2+}$ probably occurred, as suggested by the positively (Cu^{+} and Ag^{+}) vs. Ga^{3+} correlation (9d) (Bonnet et al., 2016).

Some studies show that Tl is generally enriched in Ge-rich deposits, due to the positive correlation between these two elements (Cook et al., 2009). The fluid rich Ge may also affect Tl enrichment (Fig. 9e). For the Baisong sphalerite, the Ge content is much higher than that of Tl, and whether Ge could be through coupled substitution with Tl needs further study. In low-temperature hydrothermal systems, Tl and Fe have similar geochemical behaviors, and Tl is commonly enriched in Fe-rich sulfides (e.g., pyrite) (Tu et al., 2004; Hu et al., 2019). Cook et al. (2009) proposed the coupled substitution of Fe and Ge through $2Fe^{2+}+Ge^{4+} \leftrightarrow 4Zn^{2+}$. Similar Fe vs. Ge correlation is observed in our samples, indicating that Fe could strongly affect Ge enrichment in sphalerite (Fig. 9f). It is noteworthy that sphalerite in the WHEG ore belt is generally Ge rich: Germanium enrichment in the Niujiaotang sphalerite (avg. 85 ppm) was interpreted to be related to $2Cu^{+}+Ge^{4+} \leftrightarrow 3Zn^{2+}$ (Ye et al., 2011), whilst that in the Dadongla sphalerite (avg. 600 ppm) may be caused by $2Zn^{2+} \leftrightarrow Ge^{4+}+\square$ (vacancy) (Hu et al., 2020a; Hu et al., 2020b). This suggests a variety of Ge enrichment mechanisms for the sphalerite in the WHEG belt.

5.2. Physicochemical conditions during sulfide deposition

The sphalerite trace element compositions are related to its deposition environments (e.g., redox and temperature) and ore-forming fluid composition (Kelley et al., 2004; Pfaff et al., 2011; Frenzel et al., 2016; Wei et al., 2021 and references therein). GGIMFis sphalerite geothermometer by Frenzel et al. (2016) was used here, which yielded temperature of 67–117°C (mean 92°C) for Sp I, 80–128°C for Sp II (mean 104°C), 127–164°C for Sp III (mean 146°C), and 97–141°C (mean 119°C) for Sp IV (Table 3). All in all, the mineralization temperature of Baisong ranges from 92 to 146°C, resembling typical MVT ore-forming temperature (90–150°C) (Leach et al., 2005). Therefore, we suggested that the Baisong sphalerite was formed under low temperature (highest during Sp III formation).

Iron incorporation into the sphalerite crystal lattice is strongly influenced by temperature, sulfur fugacity (fS_2), and oxygen fugacity (fO_2) (Hutchison and Scott, 1983; Kelley et al., 2004). Sphalerite chemistry could reflect the ore-forming fluid temperature and fS_2 evolution (Frenzel et al., 2021). Average fS_2 (based on GGIMFis temperature and sphalerite Fe content; ESM 1) is similar among the four ore stages, i.

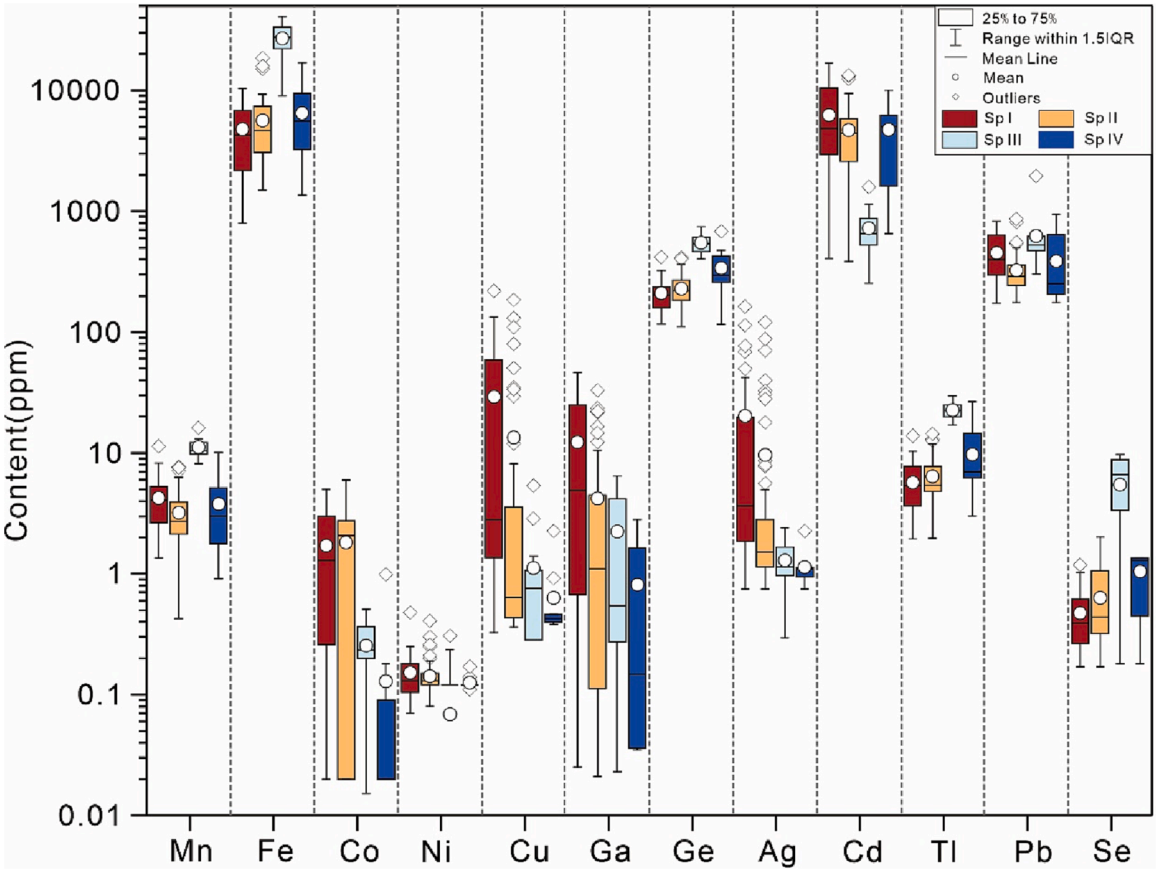

Fig. 6. Boxplots of trace elements in the four sphalerite types from Baisong. Upper and lower thresholds are 95%. The upper and lower margin of the box represent the upper 75% and 25% of the data. Mean and median values are shown as solid white circles and solid black lines, respectively.

Table 2
In situ S isotopic composition for the four types of sphalerite and two types pyrite from the Baisong Zn–Pb deposit determined by LA-MC-ICPMS.

Sample	analysis spot	δ34Sv-CDT(‰)	S.D.
Sp I(n = 4)	1-2bSpI-1	25.6	0.1
	1-1bSpI-2	24.8	0.1
	1-1aSp-I-3	25.8	0.1
	1-2aSpI-4	27.8	0.1
Sp II(n = 4)	1-2bSpII-1	26.9	0.1
	1-1bSpII-2	26.5	0.1
	1-1bSp-II-3	27.0	0.1
	1-2aSpII-2	28.0	0.1
Sp III(n = 3)	1-1aSpIII-1	31.0	0.1
	1-1aSp-III-2	31.5	0.1
	1-1bSpIII-3	32.5	0.1
Sp IV(n = 3)	1-1bSpIV-1	25.7	0.1
	1-1bSp-IV-2	29.8	0.1
	1-1bSpIV-3	28.6	0.1
Py I(n = 3)	1-1bPyI-1	46.3	0.1
	1-1bPyI-2	35.3	0.1
	1-1bPyI-3	34.2	0.1
	1-1aPyII-1	27.8	0.1
Py II(n = 5)	1-1aPyII-2	29.1	0.1
	1-1aPyII-3	30.1	0.1
	1-1aPyII-4	23.9	0.1
	1-1aPyII-5	22.5	0.1

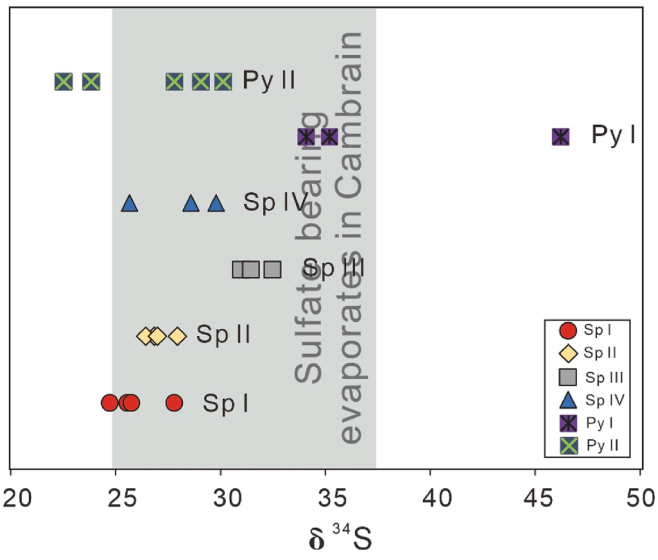

Fig. 7. δ^{34} S histogram for the various ore minerals (a) and distribution of sulfide δ^{34} S values (b) from the different ore stages at Baisong.

e., dfS_2 = -0.11 (Sp I), +0.07 (Sp II), +0.00 (Sp III), and + 0.42 (Sp IV). Higher FeS content (mol.%) in Sp III than that of Sp I–II and Sp IV (ESM 1) suggests that temperature and fS_2 have a coordinated variation during the Sp III deposition (Wei et al., 2021).

The Mn content in sphalerite is affected by redox conditions (Bernardini et al., 2004; Kelley et al., 2004): Mn tends to enter sphalerite as MnS (rather than forming Mn oxides) under reducing conditions (Vaughan and Craig, 1997), leading to high Mn content in sphalerite (Kelley et al., 2004). At Baisong, the median Mn content of Sp III (11.1 ppm) is distinctly higher than that of Sp I (4.25 ppm), SpII (3.21 ppm), and Sp IV (3.78 ppm) (Fig. 6), indicating more reducing conditions during the Sp III deposition.

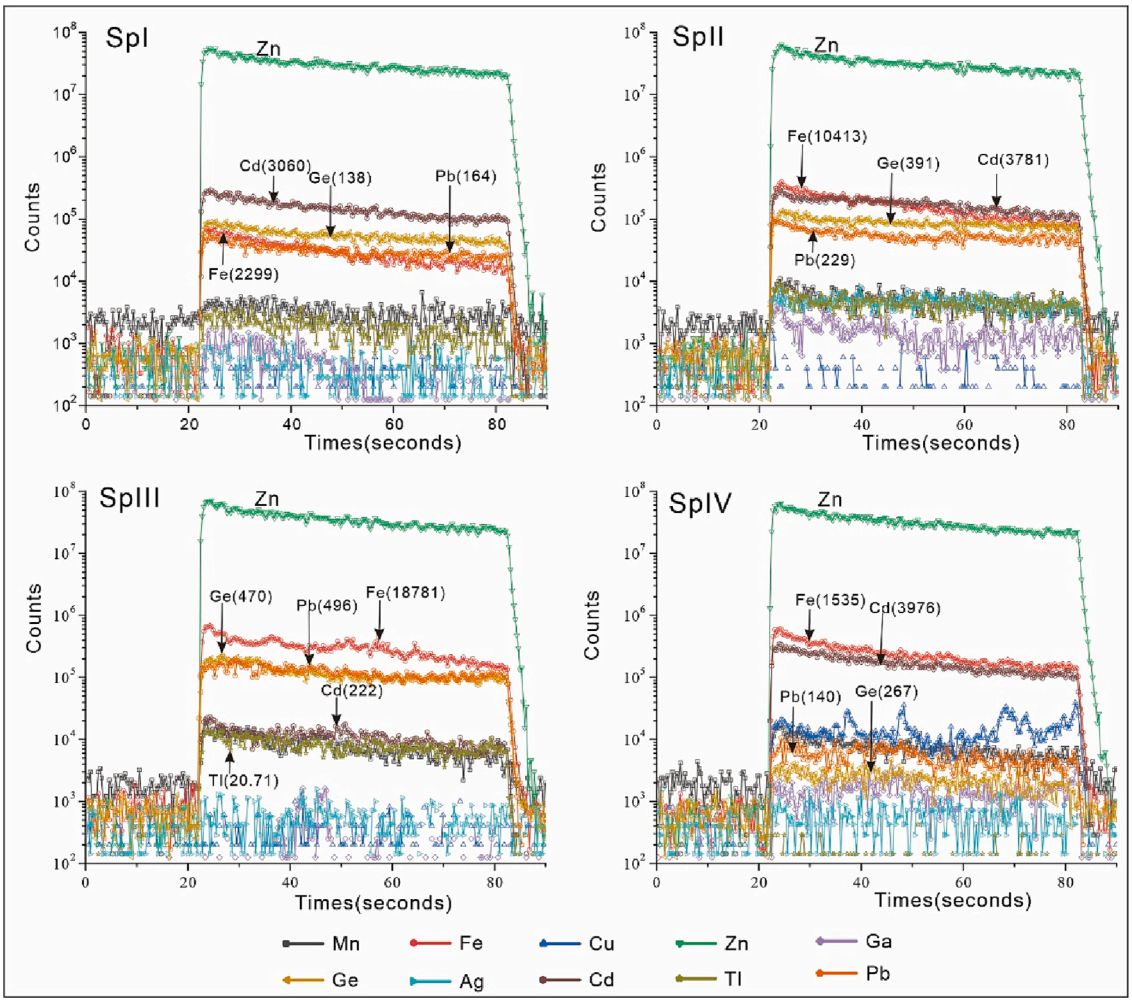

Fig. 8. Representative LA-ICP-MS time-resolved signal profiles of selected elements from the Baisong sphalerite.

Based on experimental study, Pattrick et al. (1993) reported major pH influence on the ore-forming fluid Cd-Fe-Cu-In contents. In the Baisong sphalerite, Sp III has lower Cd-Cu but higher Fe contents than Sp I-II and Sp IV (Fig. 6), which could be explained by the different fluid pH. Marcasite formation commonly indicates acidic ore fluids (pH < 4–5; Murowchick and Barnes, 1986; Kitchaev and Ceder, 2016; Luo et al., 2022). It is noteworthy that marcasite commonly overgrow with Sp I (Fig. 4b), and pyrite is often associated with Sp III (Fig. 4d). The Cd-Fe-Cu contents and microscopic observation suggest increasing pH during the Sp III formation.

5.3. Source and formation mechanism of sulfur

$\delta^{34}S$ value of the Baisong sulfides (= +22.5 to + 46.3‰) are much higher than 15‰ (Fig. 7), reflecting $\delta^{34}S$-rich fluids typical of marine sulphates (Seal, 2006). The S-bearing minerals in the Baisong deposit are mainly sulfides (sphalerite, pyrite and galena) and sulfate is largely absent (Figs. 3 and 4). Coexisting sulfides have $\delta^{34}S$ value decreasing in the order of $\delta^{34}S_{pyrite} > \delta^{34}S_{sphalerite}$, suggesting that the reduced sulfur in the ore-forming fluids may have reached thermodynamic equilibrium (Ohmoto and Rye, 1979; Ohmoto, 1986). This indicates that the sulfide $\delta^{34}S$ values at Baisong can approximate the ore-forming fluid $\delta^{34}S_{\Sigma S}$ value (Ohmoto, 1972; Seal, 2006). The Baisong sulfide $\delta^{34}S$ values (+22.5 to + 46.3‰, avg. + 29.1‰; Table 2) is indicative of a heavy S-isotope fluid source. Such $\delta^{34}S$ is much higher than that of magmatic sulfur (~0‰; Ohmoto and Rye, 1979; Chaussidon et al., 1989), but overlap with the Ediacaran-Cambrian marine sulfates (+25 to + 35‰; Claypool et al., 1980) and Cambrian sulfate-bearing evaporites in the region (+24.8 to + 37.30‰; Zhou et al., 2016; Wei et al., 2017; Hu et al., 2022). We therefore suggest that the Cambrian sulfate-bearing evaporites are a potential ore sulfur source at Baisong.

Sulfates (SO_4^{2-}) can be reduced to S^{2-} via bacterial sulfate reduction (BSR: $\Delta\ ^{34}S_{sulfate\ -\ sulfide}$ = 40-60‰) or thermochemical sulfate reduction (TSR: $\Delta\ ^{34}S_{sulfate\ -\ sulfide}$ = ~15 ± 5‰; Basuki et al., 2008; Luo et al., 2020; de Oliveira et al., 2019). The upper temperature limit of effective BSR is about 30 to 40 ℃ (Jørgensen et al., 1992), and BSR would produce sulfate–sulfide fractionation of 15 to 60‰ (Goldhaber and Kaplan, 1975) and negative $\delta^{34}S$ value for reduced sulfur. At Baisong, the $\delta^{34}S$ variation from Sp I to Sp IV and from Py I to Py II is strongly positive (from + 22.5 to + 46.3‰). The sphalerite formation temperature at Baisong is above 100℃ (Table 3), precluding BSR for the S^{2-} formation. The optimal temperature of TSR is generally > 120 ℃, and it produces sulfate–sulfide fractionation from 0 to 15‰ (Goldhaber and Kaplan, 1975; Ohmoto and Rye, 1979), corresponding to the observed S isotopic range at Baisong. Meanwhile, organic matter in the ore host (Huang, 2003) may have served as a reductant for the TSR. Hence, H_2S could be formed from sulfates via TSR, as expressed by $SO_4^{2-} + 2CH_2O = H_2S + 2HCO_3^{2-}$ or $SO_4^{2-} + 2C = S^{2-} + 2CO_2$, $SO_4^{2-} + CH_4 = H_2S + CO_2 + H_2O$ (Machel et al., 1995).

5.4. Crystal-scale S isotope and trace element coupling

The Baisong sphalerite samples shows a clear coupling (Fe, Pb, Ge, Tl, Mn vs. $\delta^{34}S$, Fig. 10a) and decoupling (Cd, Ag, Ga, Cu vs. $\delta^{34}S$,

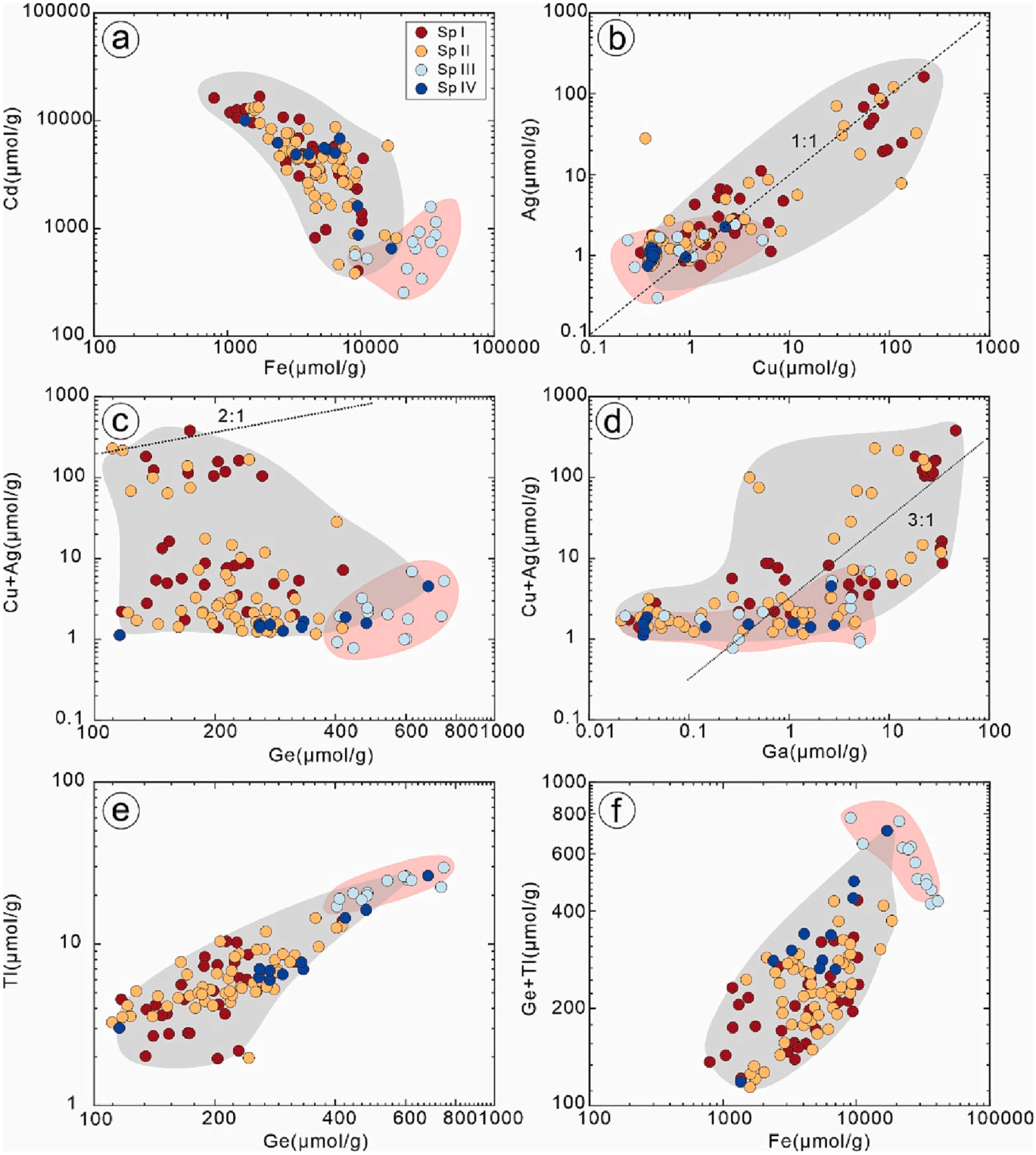

Fig. 9. Trace element binary plots for the Baisong sphalerite: (a) Fe vs. Cd, (b) Cu vs. Ag, (c) Ge vs. (Cu + Ag), (d) Ga vs. (Cu + Ag), (e) Ge vs. Tl and (f) Fe vs. (Ge + Tl).

Fig. 10b) in a crystal scale. Considering that the reduced sulfur is derived from the same source, other factors (temperature, pressure, pH, fO_2, fluid chemistry, crystal structure) responsible for precipitating sphalerite can significantly influence the sulfide S isotopic compositions (Ohmoto, 1972; O'Neil, 1986), among which temperature and fluid chemistry are the most important (Seal, 2006). The Baisong sphalerite-forming temperature (64 to 182 °C; Table 3) indicates appreciable temperature fluctuations during the sulfide precipitation. Luo et al. (2020) suggested that the S isotopic fractionation between H_2S and ZnS is very small (<1.0‰) in this temperature range.

Temperature is unlikely a major factor for the observed $\delta^{34}S$ variation. The calculations submitted by Ohmoto (1972) suggest that within the sphalerite stability field, changes in pH and fO_2 would have insignificant influence on $\delta^{34}S$ variation (~0.5‰). Thus, the Baisong

Table 3
Calculated temperature of sphalerite using GGIMFis for the Baisong deposit.

Sphalerite Type	Temperatur)(℃) range	Mean	Mn (ppm)	Fe (wt%)	Ga (ppm)	Ge (ppm)	In (ppm)
Sp I	66–117	91.8	4.25	0.48	12.3	210	0.02
Sp II	80–128	104	3.21	0.56	4.22	228	0.02
Sp III	127–164	146	11.1	2.69	2.25	548	0.02
Sp IV	97–141	119	3.78	0.65	0.81	338	0.01

sphalerite $\delta^{34}S$ variation may have mainly inherited from the fluid $\delta^{34}S$ composition. Recent studies on the Nayongzhi MVT Pb-Zn deposit (South China) showed that the $\delta^{34}S$ value of zoned sphalerite is mainly controlled by the fluid $\delta^{34}S$ composition, rather than by changes in temperature, pH, and/or fO_2 (Wei et al., 2021). Wei et al. (2021) suggested the lack of correlation between trace elements and $\delta^{34}S$ value indicates episodic ore-forming fluid influx and mixing with the wallrock-derived, reduced sulfur-rich fluids. However, some trace elements (e.g., Fe, Pb, Ge, Tl, Co and Mn) are enriched in the sphalerite core with relatively heavy S isotopes, while Ga-Cd-Sb are enriched in the bands with light sulfur isotopes from his zone sphalerite samples that is same to our investigation in Baisong deposit (Fig. 10). Therefore, in addition to episodic ore fluid influx and mixing with the reduced sulfur-rich fluid, other factors (e.g., sulfurophilic behavior of valence elements) may have contributed to the coupling behavior of sulfur isotopes and trace elements. Fe^{2+}(1.532), Ge^{4+}(1.9), Tl^{3+}(1.48), and Mn^{2+}(1.5) are more electronegative than Cd^{2+}(1.4), Cu^{2+}(1.31), Ag^{+}(1.23), and Ga^{3+}(1.2) (Pauling, 1960; Dian, 2005), which suggests that Fe, Ge, Tl, and Mn are more likely to bind to sulfur. The coupling behavior between S isotope and trace element still needs to be further explored.

5.5. Pb-Zn sulfide deposition process

Wei et al. (2020) suggested that dark colloform sphalerite was produced by rapid mixing of sufficient reduced sulfur with metal-rich fluids at the Wushihe Pb-Zn deposit (South China). SEM imaging shows that the dark colloform sphalerite contains abundant carbonate inclusions (Wei et al., 2021). The Baisong Sp I is porous and dark-colored colloform (Fig. 4b), similar to the Wushihe sphalerite, suggesting that they have undergone similar formation process. The above discussion suggests that SpI (which commonly overgrows with marcasite) was formed in an acidic environment, i.e., rapid mineral precipitation and acidic fluids could be key factors for sphalerite colloidal texture formation.

There was no significant change in temperature, fS_2 (ESM 1), and $\delta^{34}S$ value (Table 2) during the transition from colloform Sp I to sector-zoned Sp II. It is thus likely caused by the changes of precipitation conditions, including pH, and decrease in oversaturation and precipitation rate (Beaudoin, 2000; Pfaff et al., 2011; Luo et al., 2022). During successive mineralizing pulses or cycles, fast mineral growth rate could form acicular or colloform sphalerite and took up large amounts of trace metals, whereas the residue metals in the ore-forming fluids would precipitate to form euhedral sphalerite grains due to the lower growth rate (Lorens 1981; Barker and Cox 2011; Wei et al., 2021; Luo et al., 2022). In view of the decreasing Mn-Cu-Ga-Ag-Ca-Pb contents from Sp I

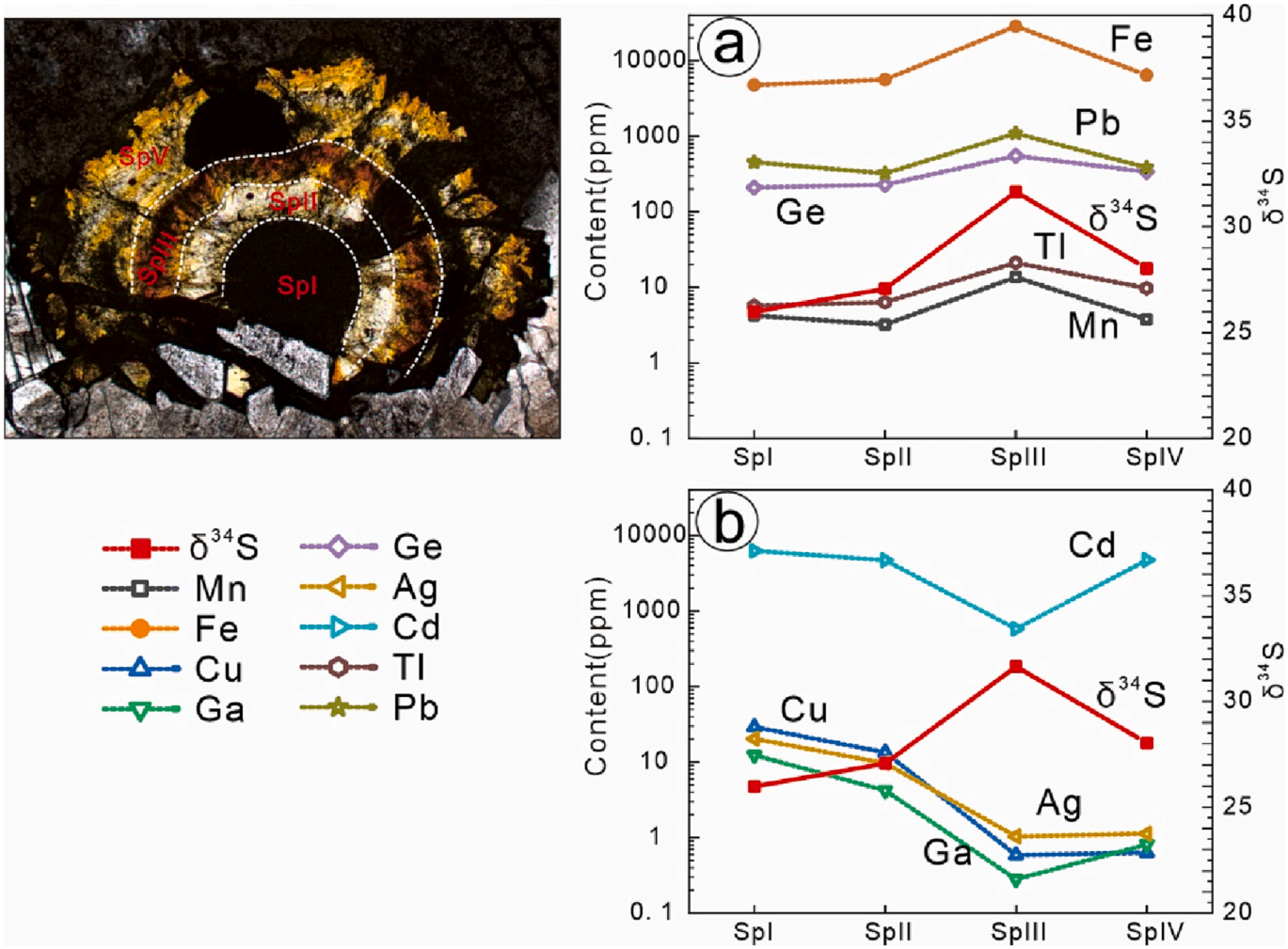

Fig. 10. Detailed traverses on the four types of sphalerites from Baisong deposit, showing the intragrain variation of trace elements and sulfur isotopes.

to II with the absence of marcasite in Sp II, we consider that the Sp II deposition is largely controlled by the decrease in oversaturation and precipitation rate, as well as ore-forming fluid pH changes. Sp III has a higher Fe-Mn-Ge-Tl and $\delta^{34}S$ but lower Ga-Ag-Cu contents than Sp II. Petrogenetic observation shows that Sp III usually closely overgrow with pyrite (Fig. 4d-e). This could be explained by: i) pre-existing pyrite and sediments as the potential source for the subsequent local hydrothermal mineralization (Gu et al., 2007; Li, 2018; Zhang et al., 2022); ii) changes in precipitation environments and fluid compositions (Roedder, 1968; Beaudoin, 2000; Pfaff et al., 2011; Wei et al., 2021; Luo et al., 2022). Zhang et al. (2022) reported higher Fe-Mn contents in early sphalerite derived from *syn*-sedimentary to early-diagenetic mineralization at the Qixiashan deposit, South China. The Cambrian host rocks in many Pb-Zn deposits in the WHEG contain pyrite with high sulfur isotopic values (Zhou et al., 2016; Wei et al., 2017; Li, 2018). Some heavy sulfur isotope values in Py I indicate that it was formed in *syn*-sedimentary (Fig. 7). However, If Sp III in Baisong was only derived from *syn*-sedimentary to early-diagenetic pyrite, it could lead to the increase of Fe content, rather than increasing content of other elements (e.g., Ge). Sphalerite with higher Ge content may be formed under low-temperature (Frenzel et al. 2016; Bauer et al. 2019), high-fS_2 (Bonnet et al., 2017), and low-pH (Pattrick et al. 1993) conditions. Hence, we suggest that Sp III was formed under higher temperature and higher pH conditions than Sp II, and changes in precipitation environments and fluid compositions are likely the key factors in forming Sp III. The four types of sphalerites exhibits intragrain $\delta^{34}S$ variation, which is attributed to the $\delta^{34}S$ composition of H_2S in the original fluid. The Sp III-forming fluid was likely heavy sulfur-rich and of higher temperature, and Sp III precipitation occurred when the ore fluid mixed with the reduced sulfur-rich fluid. Accordingly, the formation of Sp III and Py I may have consumed minor/trace elements such as Fe-Ge-Mn-Tl-Pb in the fluids. Accompanied with the decreasing temperature, this may have resulted in the depletion of these elements in Sp IV. Py II and galena were deposited after Sp I to Sp IV (Fig. 11).

5.6. Ore genetic type

Previous studies have shown that Ge and Cd tend to be enriched in deposits associated with low-temperature hydrothermal fluids, while In is more enriched in magmatic-related deposits (Cook et al., 2009; Ye et al., 2011; Shimizu and Morishita, 2012; Frenzel et al., 2016). Variations in the sphalerite Cd-Ge-In contents are dependent on their internal geochemical behavior and the initial ore-forming fluid compositions. The high Ge-Cd and low contents of the Baisong sphalerite suggest a non-magmatic-related origin.

Cook et al. (2009) and Ye et al. (2011) have proposed several minor/trace element binary plots to decipher the different types of sphalerites. The results show that the sphalerite from magmatic-related ores (e.g., skarn, epithermal, and VMS) are characterized by high In-Co-Mn and low Cd-Ge contents (Cook et al., 2009; Ye et al., 2011), and vice versa for the sphalerite from MVT ores (Schwartz, 2000; Gottesmann and Kampe, 2007; Cook et al., 2009; Ye et al., 2011; Wen et al., 2016). At Baisong deposit, the four types of sphalerites are characterized by low Mn and high Ge concentrations, consistent with MVT sphalerite (Fig. 12). In addition, all Sp I to Sp IV exhibit $\delta^{34}S = +24.7$ to $+ 32.5‰$, typical of marine sulfate isotopic signature. Moreover, the sphalerite geothermometer shows that the Baisong sphalerite was formed at 92 to 146 ℃, similar to typical MVT ore-forming temperature (90-150℃) (Leach et al., 2005). Therefore, we suggest that the Baisong is an MVT deposit.

6. Conclusions

By studying in situ trace elements and S isotopes of sphalerite at different stages from Baisong, the following findings were obtained:

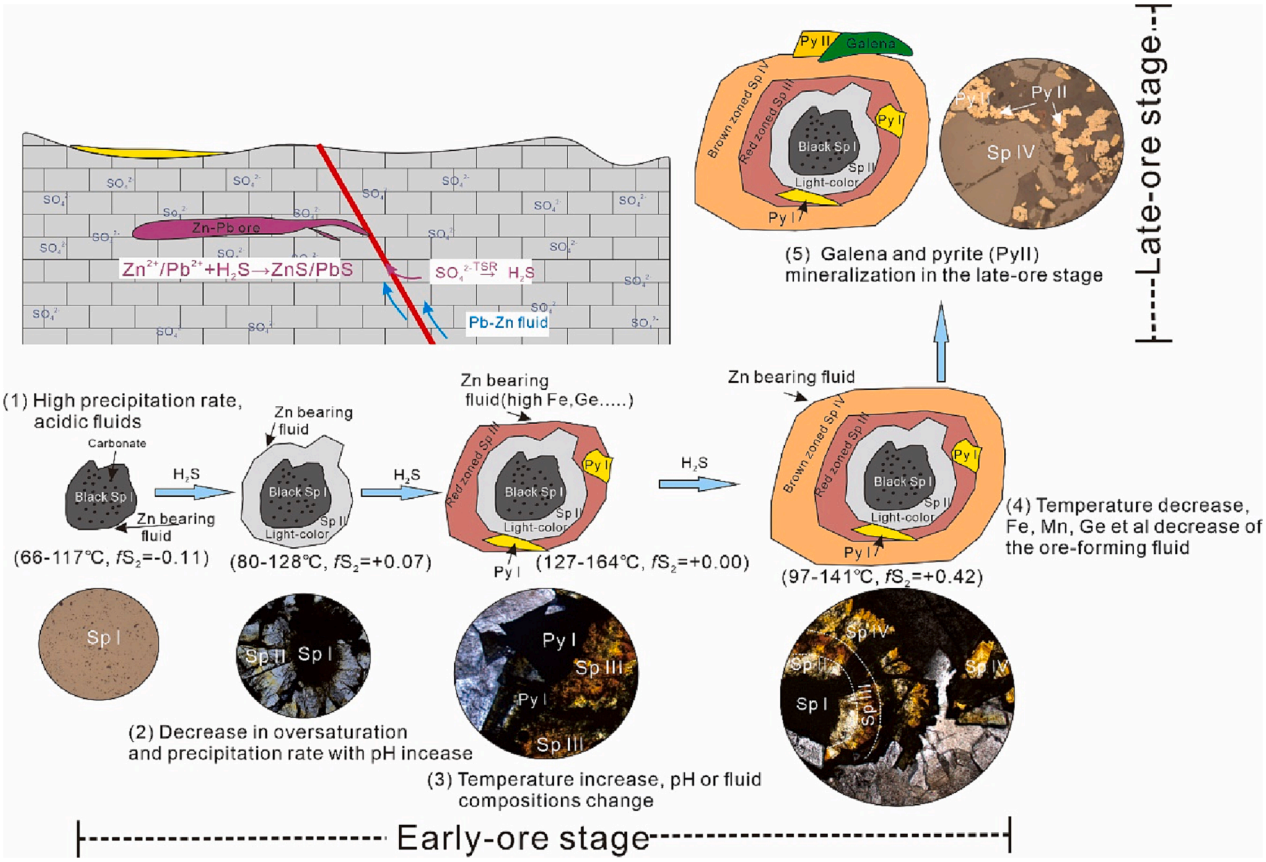

Fig. 11. Schematic diagram for the Baisong Pb-Zn mineralization.

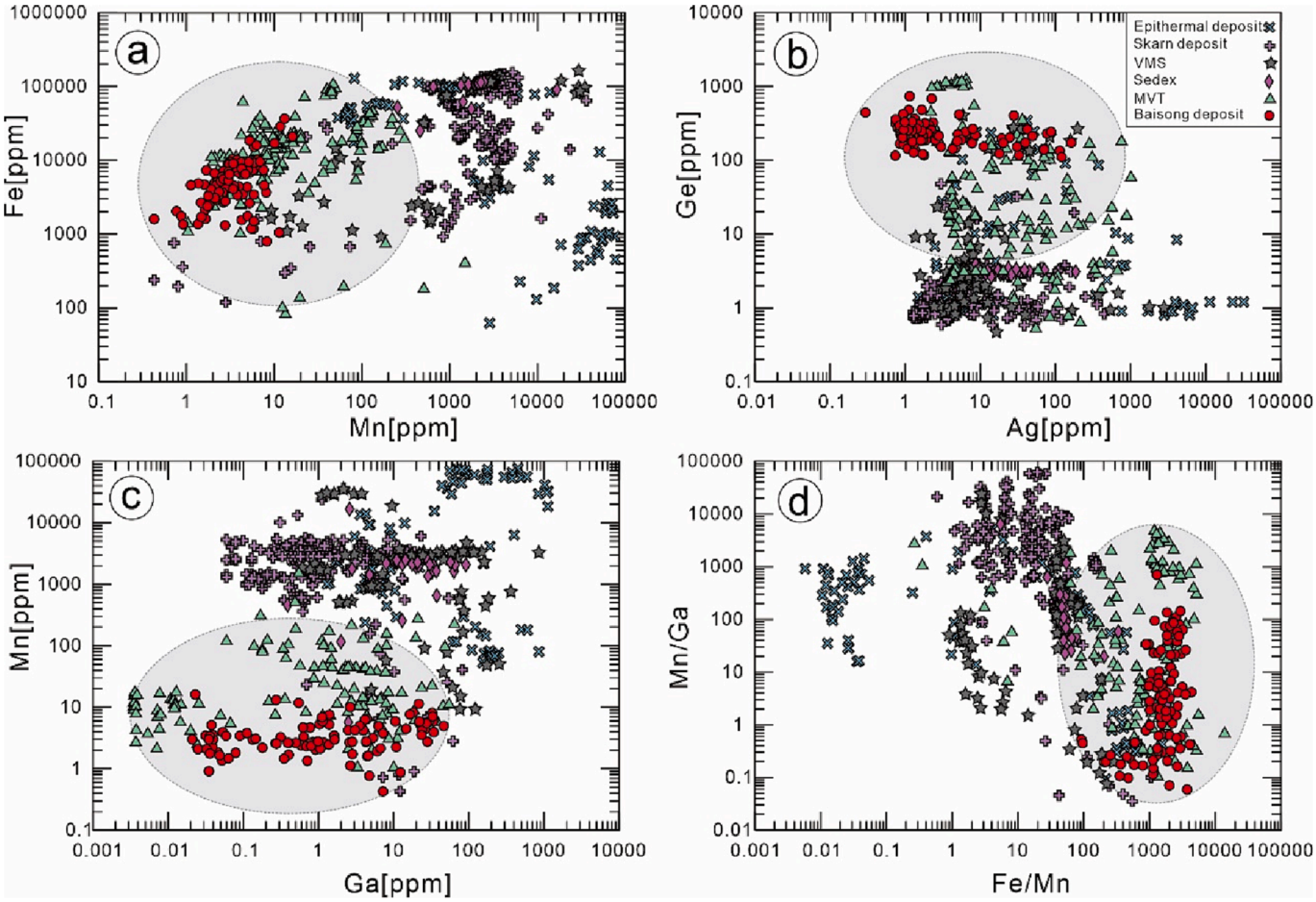

Fig. 12. Binary plots of sphalerite (a) Fe vs. Mn; (b) Ge vs. Ag; (c) Mn vs. Ga; (d) Mn/Ga vs. Fe/Mn from the Baisong deposit and major MVT, VMS, epithermal, skarn, SEDEX deposits in China, NE Europe, Canada, USA, Mexico and Japan. Data are from Cook et al. (2009), Ye et al. (2011), Ye et al. (2016) and Hu (2021).

(1) The sphalerite color is mainly controlled by the Fe content. The Fe content strongly affects the Ge-Tl enrichments in the Baisong sphalerite.
(2) Sphalerite may have precipitated under low-temperature, stable fS_2, and relatively reducing conditions. The physicochemical conditions likely changed slightly during Sp III deposition, featured by temperature and pH increase and oxygen fugacity decrease.
(3) The sulfate-bearing evaporites in Cambrian marine sedimentary rocks may have been the sulfur source for Baisong, with thermochemical sulfate reduction (TSR) playing a critical role.
(4) Sp I was formed from acidic fluids under high precipitation rate; Sp II was formed by decrease in oversaturation and precipitation rate with pH variation; Changes in precipitation environments and fluid compositions are the key in forming Sp III. Other factors (incl. sulfurophilic behavior of valence elements) contribute to the coupling of sulfur isotopes and trace elements. The formation of Sp III and Py I may have consumed Fe-Mn-Pb-Ge-Tl in the ore fluids, accompanied with the decrease of temperature, resulting in those elements depleted in Sp IV.
(5) Sphalerite from Baisong exhibit Ge-Fe enrichments and Mn depletion, similar to that of sphalerite from MVT deposits. The trace element compositional features reflect that the Baisong deposit is of MVT.

Declaration of Competing Interest

The authors declare that they have no known competing financial interests or personal relationships that could have appeared to influence the work reported in this paper.

Data availability

No data was used for the research described in the article.

Acknowledgements

This research project was jointly supported by the National Natural Science Foundation of China (42173025, 92162218), the Guizhou Science and Technology Planning Project ([2022] ZD002) and the China Postdoctoral Science Foundation (2022M710914). We thank Drs. Dai Zhihui and Dong Shaohua for helping with the LA-ICPMS and SEM analyses. We are grateful to the Editor-in-Chief and anonymous reviewers for their insightful comments.

Appendix A. Supplementary data

Supplementary data to this article can be found online at https://doi.org/10.1016/j.oregeorev.2023.105529.

References

An, Y.-L., Luo, K., Zhou, J.-X., Nguyen, A.i., Lu, M.-D., Meng, Q.-T., An, Q.i., 2022. Origin of the Devonian carbonate-hosted Banbianjie Ge-Zn deposit. Ore Geol. Rev. 142, 104696.
Bao, Z.A., Chen, L., Zong, C.L., Yuan, H.L., Chen, K.Y., Dai, M.L., 2017. Development of pressed sulfide powder tablets for in situ sulfur and lead isotope measurement using LA-MC-ICP-MS. Int. J. Mass Spectrom. 421, 255–262.

Barker, S.L., Cox, S.F., 2011. Oscillatory zoning and trace element incorporation in hydrothermal minerals: insights from calcite growth experiments. Geofuids 11, 48–56.
Barrie, C.D., Boyce, A.J., Boyle, A.P., Williams, P.J., Blake, K., Wilkinson, J.J., Lowther, M., McDermott, P., Prior, D.J., 2009. On the growth of colloform textures: A case study of sphalerite from the Galmoy orebody, Ireland. J. Geol. Soc. London 166 (3), 563–582.
Barton Jr, P.B., Bethke, P.M., Roedder, E., 1977. Environment of ore deposition in the Creede Mining district, San Juan Mountains, Colorado: Part III. Progress toward interpretation of the chemistry of the ore-forming fluid for the OH Vein. Econ. Geol. 72, 1–24.
Barton, P.B., Bethke, P.M., 1987. Chalcopyrite disease in sphalerite; pathology and epidemiology. Am. Mineral. 72, 451–467.
Basuki, N.I., Taylor, B.E., Spooner, E.T.C., 2008. Sulfur isotope evidence for thermochemical reduction of dissolved sulfate in Mississippi valley-type zinc-lead mineralization, Bongara Area, Northern Peru. Econ. Geol. 103 (4), 783–799.
Bauer, M.E., Burisch, M., Ostendorf, J., Krause, J., Frenzel, M., Seifert, T., Gutzmer, J., 2019. Trace element geochemistry of sphalerite in contrasting hydrothermal fluid systems of the Freiberg district, Germany: insights from LA-ICP-MS analysis, near infrared light microthermometry of sphalerite-hosted fluid inclusions, and sulfur isotope geochemistry. Miner. Deposita 54 (2), 237–262.
Beaudoin, G., 2000. Acicular sphalerite enriched in Ag, Sb, and Cu embedded within color-banded sphalerite from the Kokanee Range, British Columbia. Canada. Can Mineral. 38 (6), 1387–1398.
Belissont, R., Boiron, M.C., Luais, B., Cathelineau, M., 2014. LA-ICP-MS analyses of minor and trace elements and bulk Ge isotopes in zoned Ge-rich sphalerites from the Noailhac-Saint-Salvy deposit (France): insights into incorporation mechanisms and ore deposition processes. Geochim. Cosmochim. Acta 126, 518–540.
Bernardini, G.P., Borgheresi, M., Cipriani, C., Di Benedetto, F., Romanelli, M., 2004. Mn distribution in sphalerite: an EPR study. Phys. Chem. Miner. 31 (2), 80–84.
Bonnet, J., Mosser-Ruck, R., Caumon, M.-C., Rouer, O., Andre-Mayer, A.-S., Cauzid, J., Peiffert, C., 2016. Trace Element Distribution (Cu, Ga, Ge, Cd, and Fe) in Sphalerite from the Tennessee Mvt Deposits, Usa, By Combined Empa, La-ICP-MS, Raman Spectroscopy, and Crystallography. Can. Mineral. 54 (5), 1261–1284.
Bonnet, J., Cauzid, J., Testemale, D., Kieffer, I., Proux, O., Lecomte, A., Bailly, L., 2017. Characterization of germanium speciation in sphalerite (ZnS) from Central and Eastern Tennessee, USA, by x-ray absorption spectroscopy. Minerals 7, 79.
Charvet, J., 2013. The Neoproterozoic-early Paleozoic tectonic evolution of the South China Block: an overview. J. Asian Earth Sci. 74, 198–209.
Chaussidon, M., Albarède, F., Sheppard, S.M.F., 1989. Sulfur isotope variations in the mantle from ion microprobe analyses of micro-sulfide inclusions. Earth Planet. Sci. Lett. 92, 144–156.
Chen, L., Yuan, H.L., Chen, K.Y., Bao, Z.A., Zhu, L.M., Liang, P., 2019. In situ sulfur isotope analysis by laser ablation MC-ICPMS and a case study of the Erlihe Zn-Pb ore deposit, Qinling orogenic belt, Central China. J. Asian Earth Sci. 176, 325–336.
Claypool, G.E., Holser, W.T., Kaplan, I.R., Sakai, H., Zak, I., 1980. The age curves of sulfur and oxygen isotopes in marine sulfate and their mutual interpretation. Chem. Geol. 28, 199–260.
Cook, N.J., Ciobanu, C.L., Pring, A., Skinner, W., Shimizu, M., Danyushevsky, L., Saini-Eidukat, B., Melcher, F., 2009. Trace and minor elements in sphalerite: A LA-ICPMS study. Geochim. Cosmochim. Acta 73 (16), 4761–4791.
Corbella, M., Ayora, C., Cardellach, E., 2004. Hydrothermal mixing, carbonate dissolution and sulfide precipitation in Mississippi Valley-type deposits. Mineralium Deposita 39 (3), 344–357.
Danyushevsky, L., Robinson, P., Gilbert, S., Norman, M., Large, R., McGoldrick, P., Shelley, M., 2011. Routine quantitative multi-element analysis of sulfide minerals by laser ablation ICP-MS: standard development and consideration of matrix effects. Geochemistry: Exploration. Environ. Anal. 11, 51–60.
de Oliveira, S.B., Leach, D.L., Juliani, C., Monteiro, L.V., Johnson, C.A., 2019. The Zn-Pb mineralization of Florida Canyon, an evaporite-related Mississippi Valley-type deposit in the Bongará district, northern Peru. Econ. Geol. 114, 1621–1647.
Di Benedetto, F., Bernardini, G.P., Costagliola, P., Plant, D., Vaughan, D.J., 2005. Compositional zoning in sphalerite crystals. Am. Mineral. 90, 1384–1392.
Dian, Y., 2005. A new set of electronegativities of elements in valence states. Chinese J. Inorg. Chem. 7 (21), 955–959.
Duan, Q.F., 2014. The research of metallogenic regularity of stratabound zinc-lead deposits from Sinian-Cambrian in Western Hunan and Western Hubei. Ph.D. Dissertation. China University of Geosciences, Wuhan (in Chinese with English abstract).
Frenzel, M., Hirsch, T., Gutzmer, J., 2016. Gallium, germanium, indium, and other trace and minor elements in sphalerite as a function of deposit type — A meta-analysis. Ore Geol. Rev. 76, 52–78.
Frenzel, M., Voudouris, P., Cook, N.J., Ciobanu, C.L., Gilbert, S., Wade, B.P., 2021. Evolution of a hydrothermal ore-forming system recorded by sulfide mineral chemistry: a case study from the Plaka Pb-Zn-Ag Deposit, Lavrion, Greece. Mineral Deposita 57, 417–438.
Gagnevin, D., Menuge, J.F., Kronz, A., Barrie, C., Boyce, A.J., 2012. Minor elements in layered sphalerite as a record of fluid origin, mixing, and crystallization in the Navan Zn–Pb ore deposit, Ireland. Econ. Geol. 109 (6), 1513–1528.
Goldhaber, M.B., Kaplan, I.R., 1975. Controls and consequences of sulfate reduction rates in recent marine sediments. Soil Sci. 119 (1), 42–55.
Gottesmann, W., Kampe, A., 2007. Zn/Cd ratios in calcsilicate-hosted sphalerite ores at Tumurtijn-Ovoo Mongolia. Chem. Erde 67 (4), 323–328.
Gregory, D., Meffre, S., Large, R., 2014. Comparison of metal enrichment in pyrite framboids from a metal-enriched and metal-poor estuary. Am. Mineral. 99 (4), 633–644.
Gu, L., Khin Zaw, Hu, W., Zhang, K., Ni, P., He, J., Xu, Y., Lu, J., Lin, C., 2007. Distinctive features of Late Paleozoic massive sulfide deposits in South China. Ore Geol. Rev. 31 (1-4), 107–138.
Hu, Y.S., Ye, L., Huang, Z.L., Li, Z.L., Wei, C., Danyushevskiy, l., 2019. Distribution and existing forms of trace elements from Maliping Pb-Zn deposit in northeastern Yunnan, China: A LA-ICPMS study. Acta Petrol. Sin. 35 (11), 3477–3492 in Chinese with English Abstract.
Hu, Y.S., Ye, L., Wei, C., Li, Z.L., Huang, Z.L., Wang, H.Y., 2020a. Trace Elements in Sphalerite from the Dadongla Zn–Pb Deposit, Western Hunan-Eastern Guizhou Zn–Pb Metallogenic Belt, South China. Acta Geol. Sin. (Engl. Ed.) 94, 2152–2164.
Hu, Y.S., Ye, L., Wei, C., Huang, Z.L., Wang, H.Y., 2020b. REE geochemistry of the hydrothermal calcites from the Huayuan orefield, in the western Hunan, China. Acta Mineral. Sin. 40 (4), 441–449 in Chinese with English Abstract.
Hu, Y.S., Ye, L., Huang, Z.L., Wei, C., Wu, T., Xiang, Z.Z., Liu, S.Y., Li, Z.L., 2022. Genetic model for early Cambrian reef limestone-hosted Pb-Zn deposits in the world-class Huayuan orefield, South China: New insights from mineralogy, fluorite geochemistry and sulfides in situ S-Pb isotopes. Ore Geol. Rev. 141, 104682 https://doi.org/10.1016/j.oregeorev.2021.104682.
Hu, R.Z., Zhou, M.F., 2012. Multiple Mesozoic mineralization events in south China: An introduction to the thematic issue. Miner. Deposita 47 (6), 579–588.
Huang, Y.C., 2003. On Geological Characteristics and Mineralization-controlling conditions of the Baisong Lead-Zinc Deposit, Kaili. Guizhou. Guizhou Geology. 20, 35–40 in Chinese with English abstract.
Huang, Z.L., Chen, J., Han, R.S., Li, W.B., Liu, C.Q., Zhang, Z.L., Ma, D.Y., Gao, D.R., Yang, H.L., 2004. Geochemistry and ore-formation of the Huize giant lead-zinc deposit, Yunnan Province, China: Discussion on the relationship between Emeishan flood basalts and lead-zinc mineralization. Geol. Pub. House, Beijing, 1–154 (in Chinese).
Hutchison, M.N., Scott, S.D., 1983. Experimental calibration of the sphalerite cosmobarometer. Geochim. Cosmochim. Acta 47, 101–108.
Jin, Z.G., Zhou, J.X., Huang, Z.L., Luo, K., Gao, J.G., Peng, S., Wang, B., Chen, X.L., 2016. Ore genesis of the Nayongzhi Pb-Zn deposit, Puding city, Guizhou Province, China: Evidences from S and in situ Pb isotopes. Acta Petrol. Sin. 32, 3441–3455 [in Chinese with English Abstract].
Jørgensen, B.B., Isaksen, M.F., Jannasch, H.W., 1992. Bacterial sulfate reduction above 100∘C in deep-sea hydrothermal vent sediments. Science 258 (5089), 1756–1757.
Kelley, K.D., Leach, D.L., Johnson, C.A., Clark, J.L., Fayek, M., Slack, J.F., Anderson, V. M., Ayuso, R.A., Ridley, W.I., 2004. Textural, compositional, and sulfur isotope variations of sulfide minerals in the Red Dog Zn-Pb-Ag deposits. Brooks Range, Alaska: Implications for ore formation. Econ. Geol. 99 (7), 1509–1532.
Kitchaev, D.A., Ceder, G., 2016. Evaluating structure selection in the hydrothermal growth of FeS2 pyrite and marcasite. Nat. Commun. 7, 1–7.
L'Heureux, I., 2000. Origin of banded patterns in natural sphalerite. Phys. Rev. E62, 3234–3245.
Leach, D.L., Sangster, D.F., Kelley, K.D., Large, R.R., Garven, G., Allen, C.R., Gutzmer, J., Walters, S., 2005. Sediment-hosted lead-zinc deposits: a global perspective. Econ. Geol. 100th Anniv, 561–607.
Leach, D.L., Bradley, D.C., Huston, D., Pisarevsky, S.A., Taylor, R.D., Gardoll, S.J., 2010. Sediment-hosted lead-zinc deposits in Earth history. Econ. Geol. 105 (3), 593–625.
Li, Z.X., Li, X.H., Wartho, J.A., Clark, C., Li, W.X., Zhang, C.L., Bao, C.M., 2010. Magmatic and metamorphic events during the Early Paleozoic Wuyi-Yunkai orogeny, southeastern South China: new age constraints and P-T conditions. GSA Bull. 122 (5–6), 772–793.
K. Li Metallogenic Model and Prediction of the Carbonate-Hosted Pb-Zn deposits in Western Hunan and Eastern Guizhou Province, South China 2018 China University of Geosciences Wuhan Ph.D. dissertation (in Chinese with English abstract).
Liu, W.J., Zheng, R.C., 2000. Characteristic and movement of ore-forming fluids in the Huayuan lead-zinc deposit. Mineral. Depos. 19 (2), 173–181.
Lorens, R.B., 1981. Sr, Cd, Mn and Co distribution coefficients in calcite as a function of calcite precipitation rate. Geochim. Cosmochim. Act. 45, 553–561.
Luo, K., Cugerone, A., Zhou, M.F., Zhou, J.X., Sun, G.T., Xu, J., He, K.J., Lu, M.D., 2022. Germanium enrichment in sphalerite with acicular and euhedral textures: an example from the Zhulingou carbonate–hosted Zn(–Ge) deposit, South China. Mineralium Deposita. Doi: 10.1007/s00126-022-01112-4.
Luo, K., Zhou, J.X., Huang, Z.L., Caulfield, J., Zhao, J.X., Feng, Y.X., Ouyang, H., 2020. New insights into the evolution of Mississippi Valley-Type hydrothermal system: A case study of the Wusihe Pb-Zn deposit, South China, using quartz in-situ trace elements and sulfides in situ S-Pb isotopes. Am. Mineral. 105, 35–51.
Machel, H.G., Krouse, H.R., Sassen, R., 1995. Products and distinguishing criteria of bacterial and thermochemical sulfate reduction. Appl. Geochem. 10 (4), 373–389.
McLimans, R.K., Barnes, H.L., Ohmoto, H., 1980. Sphalerite stratigraphy of the upper Mississippi Valley zinc-lead district, southwest Wisconsin. Econ. Geol. 75, 351–361.
Metcalfe, I., 2006. Palaeozoic and Mesozoic tectonic evolution and paleogeography of East Asian crustal fragments: The Korean Peninsula in context. Gondw. Res. 9 (12), 24–46.
Millet, M.A., Baker, J.A., Payne, C.E., 2012. Ultra-precise stable Fe isotope measurements by high resolution multiple-collector inductively coupled plasma mass spectrometry with a 57Fe–58Fe double spike. Chem. Geol. 304–305, 18–25.
Murakami, H., Ishihara, S., 2013. Trace elements of Indium-bearing sphalerite from tin-polymetallic deposits in Bolivia. China and Japan: A femto-second LA-ICPMS study. Ore Geol. Rev. 53, 223–243.
Murowchick, J.B., Barnes, H.L., 1986. Marcasite precipitation from hydrothermal solutions. Geochim Cosmochim Act. 50, 2615–2629.
O'Neil, J.R., 1986. Theoretical and experimental aspects of isotopic fractionation. Rev. Mineral. 16, 1–40.

Ohmoto, H., 1972. Systematics of sulfur and carbon isotopes in hydrothermal ore deposits. Econ. Geol. 67, 551–578.
Ohmoto, H., Rye, R.O., 1979. Isotopes of sulfur and carbon. In: Barnes, H.L. (Ed.), Geochemistry of hydrothermal ore deposits. Wiley, New York, pp. 509–567.
Ohmoto, H., 1986. Stable isotope geochemistry of ore deposits. In: Valley, J.W., Taylor, H.P., Jr., O'Neil, J.R. (Eds.), Stable isotopes in high temperature geological processes, 1st ed. Mineralogical Society of America, Washington D.C., Rev. Mineral. Geochem. 16, pp. 491-559.
Pattrick, R.A.D., Dorling, M., Polya, D.A., 1993. TEM study of indium bearing and copper-bearing growth-banded sphalerite. Can. Mineral. 31, 105–117.
Pauling, L. The Nature of the chemical bond. 3rd ed., 1960. New York: Cornell University Press, Ithaca N.Y., 126.
Pfaff, K., Koenig, A., Wenzel, T., Ridley, I., Hildebrandt, L.H., Leach, D.L., Markl, G., 2011. Trace and minor element variations and sulfur isotopes in crystalline and colloform ZnS: Incorporation mechanisms and implications for their genesis. Chem. Geol. 286, 118–134.
Roedder, E., 1968. The non-colloidal origin of 'colloform' textures in sphalerite ores. Econo. Geol. 63, 451–471.
Rye, R.O., Ohmoto, H., 1974. Sulfur and Carbon Isotopes and Ore Genesis: A Review. Econ. Geol. 69, 826–842.
Schneider, J., Boni, M., Lapponi, F., Bechstadt, T., 2002. Carbonate-hosted zinc-lead deposits in the Lower Cambrian of Hunan, South China: A radiogenic (Pb, Sr) isotope study. Econ. Geol. 97 (8), 1815–1827.
Schwartz, M.O., 2000. Cadmium in zinc deposits: economic geology of a polluting element. Inter. Geol. Rev. 42, 445–469.
Seal, R.R., 2006. Sulfur isotope geochemistry of sulfide minerals. Rev. Mineral. Geochem. 61 (1), 633–677.
Shimizu, T., Morishita, Y., 2012. Petrography, chemistry, and near-infrared microthermometry of indium-bearing sphalerite from the Toyoha polymetallic deposit. Japan. Econ. Geol. 107, 723–735.
Tan, J.J., Liu, C.P., Yang, H.M., Cai, Y.X., Lu, S.S., 2018. Geochronology and ore-forming material source constraints for Rouxianshan Pb-Zn deposit in Huayuan ore concentration area, western Hunan. Earth Sci. 43 (7), 2438–2448 in Chinese with English abstract.
Tu, G.Z., Gao, Z.M., Chen, J.P., 2004. Dispersed element geochemistry and metallogenic mechanism. Geological Press, Beijing.
Vaughan, D.J. and Craig, J.R., 1997. Sulfide mineral stabilities, morphologies, and intergrowth texture. Pp. 367–434 in: Geochemistry of Hydrothermal Ore Deposits—Third Edition (H.L. Barnes, editor). John Wiley, New York.
Wang, Y., Fan, W., Zhang, G., Zhang, Y., 2013. Phanerozoic tectonics of the South China Block: Key observations and controversies. Gondw. Res. 23 (4), 1273–1305.
Wang, Y.F., Yang, H.M., Liu, C.P., Cai, Y.X., Tan, J.J., Xiu, X.F., Zhang, L.G., Zhu, S.Z., 2018. Strontium and sulfur isotopic characteristics of the Tangjiazhai Pb-Zn deposit in western Hunan Province, China: Denotative significance for ore-forming materials Source. China Geol. 45, 564–572 in Chinese with English abstract.
Wei, H.T., Shao, Y.J., Xiong, Y.Q., 2017. Metallogenic model of Huayuan Pb-Zn ore field in the western Hunan Province. South China. J. Cent. South Univ. 48 (9), 2402–2413 in Chinese with English abstract.
Wei, C., Ye, L., Li, Z.L., Hu, Y.S., Huang, Z.L., Liu, Y.P., Wang, H.Y., 2020. Metal sources and ore genesis of the Wushihe Pb-Zn deposit in Sichuan, China: New evidence from in-situ S and Pb isotope. Acta Petrol. Sin. 36 (12), 3783–3796.
Wei, C., Ye, L., Huang, Z.L., Hu, Y.S., Wang, H.Y., 2021. In situ trace elements and S isotope systematics for growth zoning in sphalerite from MVT deposits: A case study of Nayongzhi, South China. Mineral. Magaz. 85, 364–378.
Wen, H., Zhu, C., Zhang, Y., Cloquet, C., Fan, H., Fu, S., 2016. Zn/Cd ratios and cadmium isotope evidence for the classification of lead-zinc deposits. Sci. Rep. 6, 25273.
Yao, W.H., Li, Z.X., 2016. Tectonostratigraphic history of the Ediacaran-Silurian Nanhua foreland basin in South China. Tectonophysics 674, 31–51.
Ye, L., Cook, N.J., Ciobanu, C.L., Yuping, L., Qian, Z., Tiegeng, L., Wei, G., Yulong, Y., Danyushevskiy, L., 2011. Trace and minor elements in sphalerite from base metal deposits in South China: A LA-ICPMS study. Ore Geol. Rev. 39 (4), 188–217.
Ye, L., Li, Z.L., Hu, Y.S., Huang, Z.L., Zhou, J.X., Fan, H.F., Danyushevsky, L., 2016. Trace elements in sulfide from the Tianbaoshan Pb-Zn deposit, Sichuan Province, China: A LA-ICPMS study. Acta Petrol. Sin. 32 (11), 3377–3393 in Chinese with English abstract.
W.D. Zhang H.T. You B. Li K.D. Zhao X.D. Chen L. Zhu Ore-forming processes of the Qixiashan carbonate-hosted Pb-Zn deposit 2022 Constraints from sulfide trace elements and sulfur isotopes. Ore Geol. Rev. South China 10.1016/j.oregeorev.2022.104786.
Zhao, G.C., 2015. Jiangnan Orogen in South China: developing from divergent double subduction. Gondw. Res. 27, 1173–1180.
Zhao, J., Zhou, M.F., Yan, D., Zheng, J., Li, J., 2011. Reappraisal of the ages of Neoproterozoic strata in South China: No connection with the Grenvillian orogeny. Geology 39 (4), 299–302.
Zhou, Y., Duan, Q.F., Chen, Y.C., Tang, J.X., Cao, L., Peng, S.G., Gan, J.M., 2016. C, O, H, S, Pb and Sr isotope constraints on the sources of metals of Huayuan Pb-Zn deposits in western Hunan. Acta Geol. Sin. 90 (10), 2786–2802 in Chinese with English abstract.
Zhou, J.X., Wang, X.C., Wilde, S.A., Luo, K., Huang, Z.L., Wu, T., Jin, Z.G., 2018a. New insights into the metallogeny of MVT Pb-Zn deposits: A case study from the Nayongzhi in South China, using field data, fluid compositions, and in situ S-Pb isotopes. Am. Mineral. 103, 91–108.
Zhou, J.X., Luo, K., Wang, X.C., Wilde, S.A., Wu, T., Huang, Z.L., Cui, Y.L., Zhao, J.X., 2018b. Ore genesis of the Fule Pb-Zn deposit and its relationship with the Emeishan Large Igneous Province: Evidence from mineralogy, bulk C-O-S and in situ S-Pb isotopes. Gondw. Res. 54, 161–179.
Zhou, J.X., Xiang, Z.Z., Zhou, M.F., Feng, Y.X., Luo, K., Huang, Z.L., Wu, T., 2018d. The giant Upper Yangtze Pb–Zn province in SW China: Reviews, new advances and a new genetic model. J. Asian Earth Sci. 154, 280–315.
Zhou, J.X., Yang, Z.M., An, Y.L., Luo, K., Liu, C.X., Ju, Y.W., 2022. An evolving MVT hydrothermal system: Insights from the Niujiaotang Cd-Zn ore field, SW China. J. Asian Earth Sci. 237, 105357.